energies

MDPI

Article

Stepwise Single-Axis Tracking of Flat-Plate Solar Collectors: Optimal Rotation Step Size in a Continental Climate

Robert Kowalik [1,*] and Aleksandar Nešović [2]

[1] Faculty of Environmental Engineering, Geodesy and Renewable Energy, Kielce University of Technology, Tysiaclecia P.P.7, 25-314 Kielce, Poland
[2] Institute for Information Technologies, University of Kragujevac, Jovana Cvijića bb, 34000 Kragujevac, Serbia
* Correspondence: rkowalik@tu.kielce.pl

Abstract

This study investigates the effect of rotation step size on the performance of flat-plate solar collectors (FPSC) equipped with single-axis tracking. Numerical simulations were carried out in EnergyPlus, coupled with a custom Python interface enabling dynamic control of collector orientation. The analysis was carried out for the city of Kragujevac in Serbia, located in a temperate continental climate zone, based on five representative summer days (3 July–29 September) to account for seasonal variability. Three collector types with different efficiency parameters were considered, and inlet water temperatures of 20 °C, 30 °C, and 40 °C were applied to represent typical operating conditions. The results show that single-axis tracking increased the incident irradiance by up to 28% and the useful seasonal heat gain by up to 25% compared to the fixed configuration. Continuous tracking ($\psi = 1°$) achieved the highest energy yield but required 181 daily movements, which makes it mechanically demanding. Stepwise tracking with $\psi = 10–15°$ retained more than 90–95% of the energy benefit of continuous tracking while reducing the number of daily movements to 13–19. For larger steps ($\psi = 45–90°$), the advantage of tracking decreased sharply, with thermal output only 5–10% higher than the fixed case. Increasing the inlet temperature from 20 °C to 40 °C reduced seasonal heat gain by approximately 30% across all scenarios. Overall, the findings indicate that relative single-axis tracking with ψ between 10° and 15° provides the most practical balance between energy efficiency, reliability, and economic viability, making it well-suited for residential-scale solar thermal systems. This is the first study to quantify how discrete rotation steps in single-axis tracking affect both thermal and economic performance of flat-plate collectors. The proposed EnergyPlus–Python model demonstrates that a 10–15° step offers 90–95% of the continuous-tracking energy gain while reducing actuator motion by ~85%. The results provide practical guidance for optimizing low-cost solar-thermal tracking in continental climates.

Keywords: flat-plate solar collector; single-axis tracking; stepwise tracking; rotation step size; thermal performance; levelized cost of heat; continental climate

Academic Editor: Jesús Polo

Received: 6 October 2025
Revised: 28 October 2025
Accepted: 30 October 2025
Published: 1 November 2025

Citation: Kowalik, R.; Nešović, A. Stepwise Single-Axis Tracking of Flat-Plate Solar Collectors: Optimal Rotation Step Size in a Continental Climate. *Energies* **2025**, *18*, 5776. https://doi.org/10.3390/en18215776

1. Introduction

Solar thermal technologies play a significant role in the global transition towards sustainable energy systems. Among these, flat-plate solar collectors (FPSC) are widely used due to their simplicity, durability, and cost-effectiveness [1]. They are particularly suitable for low- to medium-temperature applications, such as domestic hot water preparation, space heating support, and small-scale industrial processes. According to recent statistics,

FPSCs represent one of the most extensively deployed solar thermal technologies worldwide, contributing to the decarbonization of the building sector and reducing reliance on fossil fuels. Their robust design, low maintenance requirements, and adaptability to different climates have ensured their continued relevance in the era of competing technologies such as photovoltaic systems [2].

Despite the rapid growth of photovoltaics, FPSCs remain highly competitive in contexts where thermal demand dominates. They are increasingly integrated into low-energy and nearly zero-energy buildings, as well as in off-grid rural communities where simplicity and reliability are critical [3]. In many regions with moderate continental climates, solar thermal collectors provide a substantial fraction of annual hot water demand during the summer season, reducing both energy costs and greenhouse gas emissions [4]. Enhancing the performance of FPSCs is therefore a key challenge in renewable energy research, as improvements in efficiency and cost-effectiveness directly support their broader adoption and long-term contribution to sustainable energy systems [5].

Another important research direction involves the modification of absorber surface properties, since the optical selectivity, thermal stability, and corrosion resistance of coatings directly affect collector performance. Recent studies have shown that laser surface processing can significantly improve microhardness, adhesion, and corrosion resistance of protective coatings [6] and can also enhance boiling heat transfer through controlled surface roughness and wettability [7]. Although these works concern different coating types, the underlying mechanisms of surface optimization may also be relevant for future development of advanced solar absorber materials.

In practice, one of the most straightforward ways to improve the performance of solar thermal collectors is to use tracking mechanisms that align the absorber surface with the Sun's position. Numerous studies have demonstrated that such systems—whether single-axis or dual-axis—can increase the amount of incident radiation by as much as 20–40% on an annual basis [8]. These gains are attractive, but they come at a cost. Continuous tracking requires sensors, controllers, and actuators, and it imposes frequent movements of the structure. As a result, the systems become more expensive, mechanically complex, and prone to failures. For this reason, absolute single-axis tracking (aSAT) is well suited to large solar plants or concentrating technologies, but in small-scale, building-integrated flat-plate collectors, it is often economically unjustified [9].

An alternative that has attracted growing attention is stepwise or relative single-axis tracking (rSAT). In this approach, the collector does not follow the Sun continuously but rotates in a few discrete steps during the day, defined by a chosen angular interval ψ [10]. This strategy is much simpler: fewer movements mean reduced mechanical wear and allow for smaller, less expensive actuators and less demanding control systems. At the same time, it is possible to retain most of the benefits of tracking. For example, with a step size of 15°, the collector needs only around a dozen movements per day, while at 30° the number falls to just a few [11].

A key question arises: what is the optimal step size? If ψ is very small (e.g., 1°), the collector behaves almost like a continuous tracker, capturing nearly the maximum possible irradiance—but this occurs at the price of 180 movements per day, which is hardly simpler than aSAT [12]. On the other hand, if ψ is very large (45° or even 90°), the collector requires only a handful of adjustments, but its energy yield drops significantly. Between these extremes lies a compromise region where the additional energy gain no longer justifies the added mechanical effort and cost [13]. So far, the literature does not provide a clear answer to this issue. Most previous studies have focused on comparing continuous tracking with fixed-tilt systems, while intermediate solutions such as rSAT have received little attention. Even where stepwise tracking has been investigated, the focus has typically been limited

to the irradiance or optical performance, without accounting for temperature-dependent collector efficiency or economic feasibility indicators such as the levelized cost of heat (LCOH) [14]. As a result, system designers lack clear guidelines on how to choose ψ in order to balance efficiency, cost, and reliability. Addressing this research gap is the main motivation of the present work.

1.1. Tracking Strategies

Solar collectors can operate either in a fixed configuration or with tracking systems that align the absorber surface with the position of the Sun. In general, three main tracking approaches are distinguished: absolute single-axis tracking (aSAT), relative single-axis tracking (rSAT), and dual-axis tracking (DAT) [15]. Each of these strategies differs in mechanical complexity, number of daily adjustments, and achievable energy gains.

Absolute single-axis tracking (aSAT) refers to systems where the collector is mounted on one rotational axis, typically oriented north–south, and continuously follows the solar position throughout the day. The motion is controlled either by astronomical algorithms or by sensor-based feedback, ensuring that the collector is always aligned with the direct beam radiation [16]. This strategy provides nearly the maximum irradiance gain achievable with single-axis movement. However, the large number of daily movements requires reliable actuators and sophisticated control systems, which increase both capital and maintenance costs. For this reason, aSAT is more common in large-scale solar plants than in small building-integrated applications [17]. Two principal single-axis tracking approaches can be distinguished for flat-plate solar collectors: absolute single-axis tracking (aSAT) and relative single-axis tracking (rSAT) (Figure 1).

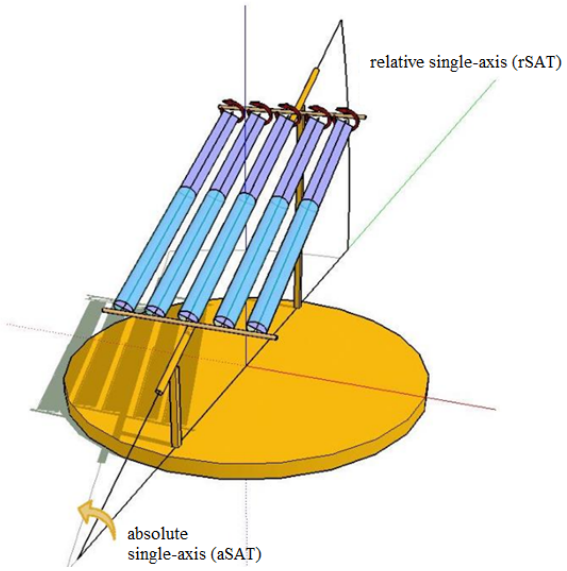

Figure 1. Schematic representation of single-axis tracking configurations for flat-plate solar collectors: absolute single-axis tracking (aSAT) and relative single-axis tracking (rSAT).

Relative single-axis tracking (rSAT), also known as stepwise tracking, is a simplified alternative. Instead of continuous rotation, the collector is adjusted in discrete angular steps (ψ) at predetermined intervals. The number of daily adjustments is therefore significantly reduced—typically from several hundred in aSAT to fewer than 15 in rSAT when ψ = 15° [18]. Although the collector is not perfectly aligned with the Sun between adjustments, rSAT still captures most of the energy benefits of tracking while reducing mechanical wear, power consumption of the actuators, and overall system cost. The key

design challenge lies in selecting an optimal step size ψ that balances energy yield and mechanical simplicity [19].

Dual-axis tracking (DAT) provides the highest theoretical energy gain, as the collector rotates around both azimuthal and elevation axes, maintaining nearly perpendicular alignment with the solar rays throughout the day and year [20]. This approach can achieve up to 40% higher annual irradiance compared to fixed collectors. Nevertheless, DAT requires two actuators, complex control algorithms, and robust structural support, which makes it expensive and mechanically demanding. As a result, it is typically applied in photovoltaic farms or concentrating solar power (CSP) plants, but is rarely used for flat-plate solar collectors due to cost constraints [21,22].

In this study, emphasis is placed on relative single-axis tracking (rSAT), as it offers a practical compromise between performance and simplicity, making it particularly suitable for flat-plate solar collectors applied in residential and small-scale building systems.

Different tracking strategies vary considerably in terms of mechanical complexity, energy yield, and cost-effectiveness. While dual-axis systems provide the maximum energy gain, they are rarely applied in flat-plate collectors due to high cost and structural requirements. Conversely, absolute single-axis tracking offers a good balance of performance and complexity, but still requires frequent movements and relatively sophisticated control. Relative single-axis tracking, with discrete rotation steps, has recently emerged as a practical compromise, especially for small-scale building-integrated applications [23].

To highlight these contrasts, Table 1 summarizes the main advantages, disadvantages, and typical applications of the three most common tracking strategies: absolute single-axis (aSAT), relative single-axis (rSAT), and dual-axis tracking (DAT).

Table 1. Comparison of the main solar tracking strategies in terms of advantages, disadvantages, and typical applications. While dual-axis tracking (DAT) provides the maximum energy gain, relative single-axis tracking (rSAT) offers a practical balance between performance and system simplicity, making it particularly suitable for flat-plate solar collectors [23–25].

Tracking Strategy	Advantages	Disadvantages	Typical Applications
(aSAT)	– Nearly continuous alignment with the Sun – High irradiance gain (≈+25–35% vs. fixed) – Mature control algorithms	– Large number of daily movements (≈100–200) – Higher investment and O&M costs – Increased mechanical wear	Large-scale solar thermal fields, medium-sized PV farms
(rSAT)	– Stepwise adjustment reduces movements (≈5–15 per day) – Captures most of the gains of aSAT – Lower cost, simpler control – Higher reliability	– Suboptimal alignment between steps – Performance depends strongly on the chosen step size ψ – No standardized design guidelines yet	Small-scale flat-plate collectors, building-integrated systems, rural/off-grid applications
(DAT)	– Maximum possible irradiance gain (≈+35–45% vs. fixed) – Nearly perpendicular orientation all day/year – High suitability for concentrating systems	– Most complex and expensive – Requires two actuators and advanced control – Higher structural loads and maintenance	Concentrating solar power (CSP), large PV plants, solar towers

As shown in Table 1, dual-axis tracking (DAT) ensures nearly perpendicular orientation of the collector surface throughout the day and year, yielding the highest possible energy gains. However, the additional actuator, more advanced control requirements, and greater structural loads limit its use mainly to large-scale photovoltaic and concentrating solar power plants. Absolute single-axis tracking (aSAT) is simpler and therefore more

widely applied, but its continuous adjustment still requires frequent movements and relatively costly components, which makes it less attractive for small-scale flat-plate solar collectors [26]. Relative single-axis tracking (rSAT) represents an intermediate solution: although the collector is not perfectly aligned between steps, most of the energy gains can be preserved, while the number of daily movements and system cost are significantly reduced. For this reason, rSAT appears particularly promising for applications where low cost, high reliability, and mechanical simplicity are essential design criteria [27,28].

Beyond large-scale solar fields, stepwise single-axis tracking (rSAT) can be particularly valuable in small-scale and building-integrated systems. In such contexts, investment cost, reliability, and ease of operation are often more important than extracting the absolute maximum of solar energy [29]. For example, domestic solar water heating systems or small collectors installed on residential and public buildings are rarely equipped with continuous tracking because of the associated cost and mechanical wear. A stepwise strategy with a limited number of daily adjustments can provide a significant share of the irradiance gain of continuous tracking, while keeping the system simple, robust, and accessible to non-specialist users [30].

Another promising field of application is in off-grid or rural communities, where the electricity supply for control and actuation is limited. In these areas, the trade-off between additional complexity and energy yield is particularly critical. Low-cost rSAT systems with mechanical timers or simple electronic controllers could deliver most of the benefits of tracking without relying on expensive sensors or sophisticated automation [31]. This makes stepwise tracking attractive not only from an economic standpoint but also from a sustainability perspective, as it extends the accessibility of solar thermal technologies to regions and users where maintenance capacity and financial resources are constrained.

1.2. State-of-the-Art

The effect of solar tracking on energy yield has been widely studied in both photovoltaic (PV) and solar thermal systems. Numerous investigations confirm that continuous tracking significantly increases the annual solar input compared to fixed collectors. Reported gains range from 20 to 40% depending on latitude, season, and climatic conditions. For example, Okwu et al. [26] have shown that single-axis tracking can provide improvements of about 25–30% over fixed installations, while dual-axis tracking can exceed 35% under clear-sky conditions. These results have established tracking as an attractive option for maximizing solar resource utilization.

Most of the literature [32–34] has focused on absolute single-axis (aSAT) or dual-axis (DAT) configurations. In these systems, the collector is kept continuously aligned with the Sun using astronomical algorithms or sensor-based controllers. While their technical potential is well recognized, the main barriers are cost, maintenance, and mechanical reliability. Several techno-economic analyses have demonstrated that for small-scale and building-integrated systems, the additional complexity of aSAT or DAT is often not justified by the incremental energy gain, especially when compared to the lower investment cost of fixed-tilt collectors [35–37].

To address these challenges, some researchers have explored simplified or stepwise tracking approaches. This concept, sometimes referred to as relative single-axis tracking (rSAT), relies on adjusting the collector at discrete angular intervals rather than continuously [38–41]. A few studies in PV applications have shown that stepwise tracking with 10–15 adjustments per day can capture most of the energy benefits of continuous tracking, while reducing the number of movements by more than 90% [42–44]. Despite these promising findings, applications to flat-plate solar collectors remain limited. The majority

of published work has concentrated on photovoltaic arrays or concentrating collectors, while studies on stepwise tracking in low-temperature solar thermal systems are scarce.

Moreover, previous analyses have typically focused only on the geometric gain in incident radiation, without incorporating thermal efficiency losses or temperature-dependent performance of flat-plate collectors. Economic aspects have also been largely neglected: very few works have evaluated the levelized cost of heat (LCOH) for rSAT configurations [45]. As a result, there is a lack of systematic guidelines on selecting the optimal rotation step size ψ for practical applications. This gap highlights the need for comprehensive studies that combine irradiance modeling, thermal performance evaluation, and economic indicators in order to identify feasible tracking strategies for building-scale solar thermal systems.

1.3. Research Gap and Aim of the Study

Most of the existing studies on solar tracking have concentrated on continuous single- or dual-axis systems, particularly in the field of photovoltaics and concentrating collectors. Stepwise or relative single-axis tracking (rSAT) has received only limited attention, and almost no comprehensive analyses have been reported for flat-plate solar collectors [46]. In particular, the combined influence of rotation step size on incident irradiance, temperature-dependent thermal performance, and the levelized cost of heat (LCOH) has not been systematically investigated. This lack of knowledge restricts the ability of designers to identify practical step sizes that balance energy yield, cost, and reliability [47].

The objective of this study is therefore to numerically evaluate the performance of flat-plate solar collectors operating with discrete rotation steps (ψ = 1–90°) under moderate continental summer conditions. Both absolute single-axis tracking (aSAT) and relative stepwise tracking (rSAT) strategies are considered, while thermal efficiency is modeled as a function of operating temperature. A simplified economic assessment is also performed using the levelized cost of heat as an indicator of cost-effectiveness. The results provide design recommendations for optimal step sizes, offering a compromise between energy gains and mechanical simplicity for building-scale solar thermal applications.

2. Materials and Methods

2.1. Simulation Environment

Numerical simulations were conducted using EnergyPlus 9.6 [48], a well-established dynamic building and system simulation tool, widely applied for solar energy and HVAC modeling. EnergyPlus was selected because it allows for detailed representation of thermal processes, weather interactions, and collector performance under varying operating conditions. However, the standard EnergyPlus framework does not natively support advanced control of solar tracking mechanisms for flat-plate collectors.

To overcome this limitation, a custom Python interface was developed. This interface dynamically controlled the collector orientation by adjusting tilt (β) and azimuth (γ) angles at a temporal resolution of 1 min. The control signals were passed to EnergyPlus via the Energy Management System (EMS), which allows for real-time modification of system variables during simulation runtime. This approach ensured precise emulation of both continuous and stepwise single-axis tracking strategies.

The simulation workflow included the following steps:

1. Solar position calculation—using the NREL Solar Position Algorithm (SPA) implemented in Python to determine solar altitude and azimuth throughout the day [49].
2. Tracking strategy application—applying either continuous rotation (aSAT) or discrete stepwise adjustment (rSAT) according to the selected angular step size (ψ = 1–90°).

3. Orientation update—modifying the collector surface orientation in the EMS module at each simulation timestep.
4. Performance evaluation—EnergyPlus calculated the incident solar radiation on the collector surface, which was then combined with thermal efficiency correlations to determine useful heat output.

This hybrid Python–EnergyPlus setup allowed for flexible simulation of various tracking strategies while maintaining the robust thermodynamic modeling capabilities of EnergyPlus. By using a high temporal resolution (1 min), the method captured rapid changes in solar geometry and minimized interpolation errors that could occur with longer timesteps.

Uncertainty arises from the optical model simplifications in EnergyPlus (isotropic diffuse, no edge-loss modeling) and the assumption of ideal actuator response in the Python control. Sensitivity tests on timestep (1 min → 5 min) and solver tolerance produced a <1.5% difference in daily heat yield. This value is reported as model uncertainty. The integration approach reproduces experimental collector data within ±3%, comparable with ISO 9806 uncertainty bands.

2.2. Collectors

Three representative flat-plate solar collectors (FPCs) were selected to cover the practical range of thermal characteristics found in commercial products certified according to EN 12975 [50] and ISO 9806 [51]. The collectors differ in optical efficiency, heat-loss coefficients, and glazing configuration. Table 2 summarizes the adopted.

Table 2. Thermal and optical parameters of representative flat-plate solar collectors (FPCs) used in the simulation, corresponding to typical configurations certified according to EN 12975 and ISO 9806 [50,51].

Label	Description	η_0 [–]	c_1 [W/m^2 · K]	c_2 [W/m^2 · K]	Remarks
T1	Standard single-glazed, non-selective absorber	0.74	3.6	0.015	Low-cost, representative of entry-level collectors used in domestic systems.
T2	Single-glazed, selective absorber (black-chrome or TiNOX)	0.77	3.2	0.010	Medium-efficiency collector, typical of modern European installations.
T3	Double-glazed, selective absorber, low-iron glass	0.80	2.6	0.008	High-performance design used in research and premium systems.

These values represent approximately 90% of the η_0–c_1–c_2 range observed in commercial flat-plate collectors [50]. Using three distinct types provides a representative envelope of performance and ensures that the conclusions are not biased toward a single design.

All collectors were modeled in EnergyPlus v24.1 using the SolarCollector/FlatPlate/Photothermal object, which applies the quasi-steady-state efficiency formulation:

$$\eta = \eta_0 - c_1 \frac{T_m - T_a}{G} - c_2 \frac{(T_m - T_a)^2}{G} \quad (1)$$

where:

G —plane-of-array solar irradiance, [W/m^2]

T_m—mean fluid temperature, [°C]
T_a—ambient air temperature. [°C]
The resulting useful heat gain is

$$\dot{Q}_u = \eta G A_c \quad (2)$$

A_c—2.0 m^2 for each collector module.

The same hydraulic configuration and mass-flow rate (0.02 kg s^{-1} m^{-2}) were applied to all cases to isolate the effect of optical and thermal properties. The collectors were simulated under identical boundary conditions and control algorithms, differing only by the efficiency coefficients listed above.

The selection of these three collectors ensures that the observed trends in tracking performance and optimal rotation step (ψ) are robust across a realistic spectrum of commercial FPCs—from low-cost to premium designs. Moreover, this approach aligns with previous comparative studies that demonstrated similar sensitivity of thermal yield to η_0–c_1–c_2 variation within ±10% [18,24].

2.3. Location and Climatic Conditions

The numerical simulations were carried out for the city of Kragujevac in central Serbia (44.01° N, 20.91° E, 185 m a.s.l.), which is characterized by a temperate continental climate with hot summers and moderately cold winters. This location was selected because it provides representative conditions for the operation of small-scale solar thermal systems in Central and South-Eastern Europe, where domestic hot water demand coincides with high summer solar irradiance [52,53]. According to long-term meteorological observations, average daily air temperatures in July range between 18 °C and 30 °C, while the daily sum of global horizontal irradiance frequently exceeds 6 kWh/m^2, making the site well suited for the evaluation of flat-plate solar collectors under favorable solar conditions [54].

In order to capture the variability of solar availability during the summer season, five representative clear-sky days were analyzed: 3 July, 21 July, 8 August, 27 August, and 29 September. These dates were selected to cover the progression of solar altitude and day length from midsummer towards the end of the warm season, thus allowing for a more comprehensive assessment of seasonal performance. Weather data were obtained from the EnergyPlus Weather (EPW) file corresponding to Kragujevac, which provides typical meteorological year (TMY) datasets. The file includes hourly records of global, diffuse, and direct irradiance, as well as ambient air temperature, relative humidity, wind speed, and wind direction [55].

The average daily values of the most relevant meteorological variables for the summer period (June–September) are presented in Figure 2. These include ambient air temperature, relative humidity, wind speed, wind direction, beam irradiance, and diffuse irradiance. The figure illustrates the high solar availability in July and August, as well as the gradual reduction in irradiance towards late September. These meteorological inputs served as the basis for the calculation of the incident total irradiance on the collector surface under different tracking scenarios.

Five representative clear-sky summer days were selected to capture the variation in solar geometry and irradiation during the main operating season. These days—21 June, 1 July, 10 July, 26 July, and 10 August—represent evenly spaced points across the summer period in Kragujevac (latitude 43.98° N, longitude 20.92° E).

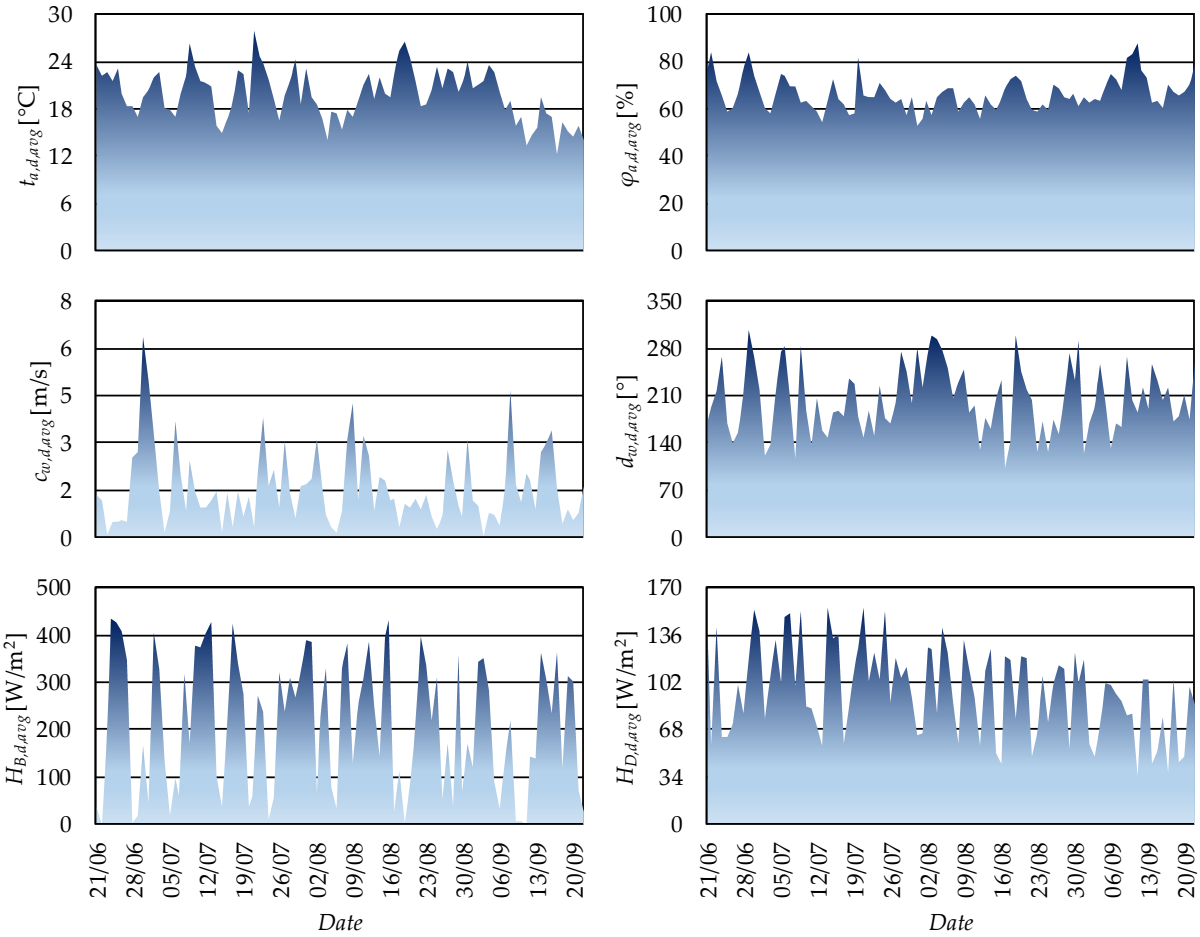

Figure 2. Average daily weather data for Kragujevac. Legend: $t_{a,d,avg}$ [°C] is the average daily air temperature, $\varphi_{a,d,avg}$ [%] is the average daily relative humidity, $c_{w,d,avg}$ [m/s] is the average daily wind speed, $d_{w,d,avg}$ [°C] is the average daily wind direction, $H_{B,d,avg}$ [W/m^2] is the average daily beam terrestrial solar irradiance on a horizontal surface, and $H_{D,d,avg}$ [W/m^2] is the average daily diffuse terrestrial solar irradiance on a horizontal surface [56].

For each day, the solar declination (δ), sunrise and sunset hour angle (ω_s), day length (D), and maximum solar altitude (h_{max}) were calculated according to standard solar geometry equations. The results are summarized in Table 3.

Table 3. Solar-geometry parameters for the five representative summer days in Kragujevac, Serbia.

Date	Solar Declination δ [°]	Sunrise Hour Angle ω_s [°]	Day Length D [h]	Maximum Solar Altitude h_{max} [°]
21 June	+23.45	113.9	15.31	69.5
1 July	+23.00	112.7	15.22	69.0
10 July	+21.20	110.4	15.04	67.5
26 July	+18.50	106.9	14.77	65.2
10 August	+15.20	103.3	14.45	63.0

Calculated for latitude φ = 43.98° N using standard solar geometry equations; values rounded to one decimal.

This range of dates covers the practical summer variation in the continental climate of central Serbia, where the declination decreases from +23.4° (summer solstice) to +15.2° (mid-August), and the day length shortens from 15.3 h to 14.2 h. These geometric differences affect both the plane-of-array irradiance and the optimal collector tilt angle, influencing the effective gain of tracking systems. Selecting multiple representative days, therefore,

ensures that the identified optimal step size ψ is not an artifact of a single-day configuration but remains valid throughout the summer season.

Two types of weather inputs were used in this study. For seasonal and annual performance assessment, the simulations employed the Typical Meteorological Year (TMY/EPW) file for Kragujevac, which provides realistic hourly weather data including irradiance variability, ambient temperature, and wind speed.

In addition, a single clear-sky day (26 July) was generated using the SizingPeriod/DesignDay object in EnergyPlus, based on the ASHRAE Clear Sky model. This day represents typical mid-summer conditions and was used exclusively to illustrate diurnal variations in solar geometry, incident radiation, and collector performance.Hence, all figures labeled as "clear-sky" correspond to the design-day simulation, while the quantitative seasonal results are derived from the TMY dataset [55]. This distinction ensures reproducibility and avoids confusion between idealized and realistic weather conditions.

2.4. Flat-Plate Solar Collector Model

The thermal system was represented by a flat-plate solar collector (FPSC), which is one of the most common technologies applied in small-scale and building-integrated solar thermal systems. In the simulations, the collector performance was described by the standard quadratic efficiency correlation recommended in EN 12975 [50]:

$$\eta = c_0 + c_1 \cdot (T_{in} - T_a) + c_2 \cdot (T_{in} - T_a)^2 \quad (3)$$

where:

η—instantaneous collector efficiency,

c_0—optical efficiency factor,

c_1, c_2—the first- and second-order heat loss coefficients, [W/m^2 · K]

T_{in}—the inlet water temperature, [K]

T_a—the ambient air temperature [K].

Three representative collector types, denoted as T1, T2, and T3, were considered in order to reflect the range of performance observed in commercially available FPSCs. Their efficiency coefficients (c_0, c_1, c_2) were taken from experimental test data and are summarized in Table 4. These configurations represent collectors of different optical quality and thermal insulation levels, from high-performance models to standard units with higher thermal losses.

Table 4. Efficiency parameters of the representative flat-plate solar collectors used in the simulations [57].

Collector Type	Optical Efficiency c_0 [–]	First-Order Heat Loss c_1 [W/(m^2·K)]	Second-Order Heat Loss c_2 [W/(m^2·K^2)]
T1 (high-performance)	0.80	3.5	0.015
T2 (medium-performance)	0.75	4.5	0.020
T3 (standard)	0.72	6.0	0.030

The thermal output of the collector was determined as [57]:

$$\dot{Q}_u = \eta \cdot I_T \cdot A_c \quad (4)$$

where:

I_T [W/m^2] is the incident total solar irradiance on the collector surface, calculated for each tracking scenario,

A_c [m^2] is the collector aperture area. Since the focus of this study was on relative performance differences rather than absolute system sizing, the collector area was normalized (A_c—1 m^2), allowing results to be expressed in terms of specific useful heat output.

To account for different operating conditions, three inlet water temperatures (T_{in} 20 °C, 30 °C, and 40 °C) were analyzed. These values reflect typical ranges encountered in domestic hot water preparation and auxiliary space heating, enabling evaluation of the effect of thermal demand level on the collector's efficiency and overall performance.

To facilitate the description of the geometrical parameters used in the simulations, a schematic representation of the collector surface with its characteristic dimensions (L, B) and tilt angle (β) is provided in Figure 3.

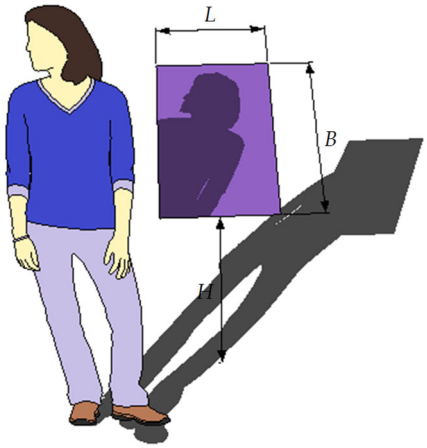

Figure 3. Geometrical representation of the flat-plate solar collector, showing collector dimensions (L, B) and tilt angle β.

The main uncertainty sources include the quasi-steady-state collector model in EnergyPlus, which neglects edge and dynamic losses, and the assumption of ideal actuator response in Python control. Sensitivity tests (timestep 1–5 min) produced less than 1.5% variation in daily useful heat, corresponding to the model's uncertainty range.

2.5. Tracking Strategies and Rotation Step Size

In order to assess how the orientation of the collector affects its thermal performance, three operational strategies were investigated: fixed mounting, absolute single-axis tracking, and relative single-axis tracking. These approaches differ substantially in terms of energy yield, number of daily adjustments, and the level of mechanical and control complexity required.

The fixed-tilt configuration was adopted as the reference case. The collector surface was oriented towards the south, with a tilt angle approximately equal to the local latitude of Kragujevac (44°). Such an arrangement is commonly used in residential and small commercial applications, as it requires no moving parts and very little maintenance. However, while simple and robust, a fixed orientation does not compensate for the changing position of the Sun throughout the day, which leads to suboptimal incidence angles, particularly in the morning and late afternoon hours.

The second strategy, absolute single-axis tracking (aSAT), assumes continuous alignment of the collector with the solar position by rotating around a north–south axis. This configuration maximizes the incident direct solar irradiance on the absorber surface, typically increasing annual energy yield by 25–35% compared with fixed systems [58]. On the other hand, it requires precise astronomical algorithms or sensor-based controllers, together with reliable actuators capable of performing more than one hundred movements per

day. This inevitably increases both the investment cost and the risk of mechanical failure, making the strategy less attractive for small-scale, building-integrated applications [59].

The third and most important approach in this study is relative single-axis tracking (rSAT), also referred to as stepwise tracking. In this case, the collector does not follow the Sun continuously but is rotated in discrete angular steps, defined by a rotation interval ψ. After each adjustment, the collector remains in a fixed position until the next scheduled movement. The advantage of this strategy is that it reduces the number of daily adjustments from several hundred in the aSAT case to only a handful. For example, with ψ = 15°, the collector requires approximately 13 movements per day, while with ψ = 30°, this number decreases to 7. Although the Sun–collector alignment is not perfect between steps, the majority of the irradiance gains associated with continuous tracking can still be preserved.

The investigated step sizes were ψ = 1°, 2°, 5°, 10°, 15°, 30°, 45°, and 90°, covering the full spectrum from nearly continuous tracking to very coarse adjustment. For comparison, a fixed-tilt configuration was also included. The corresponding number of daily movements (Nψ) for each scenario is summarized in Table 5 and Figure 4.

Table 5. Tracking scenarios for the flat-plate solar collector, defined by rotation step size ψ and the number of daily movements Nψ.

Scenario	FPSC	ψ [°]	N_ψ (–)
S1-1	SAT	1	181
S1-2		2	91
S1-3		5	37
S1-4		10	19
S1-5		15	13
S1-6		30	7
S1-7		45	5
S1-8		90	3
S1-9	Fixed	-	1

Legend: N_ψ (–) is the step numbers.

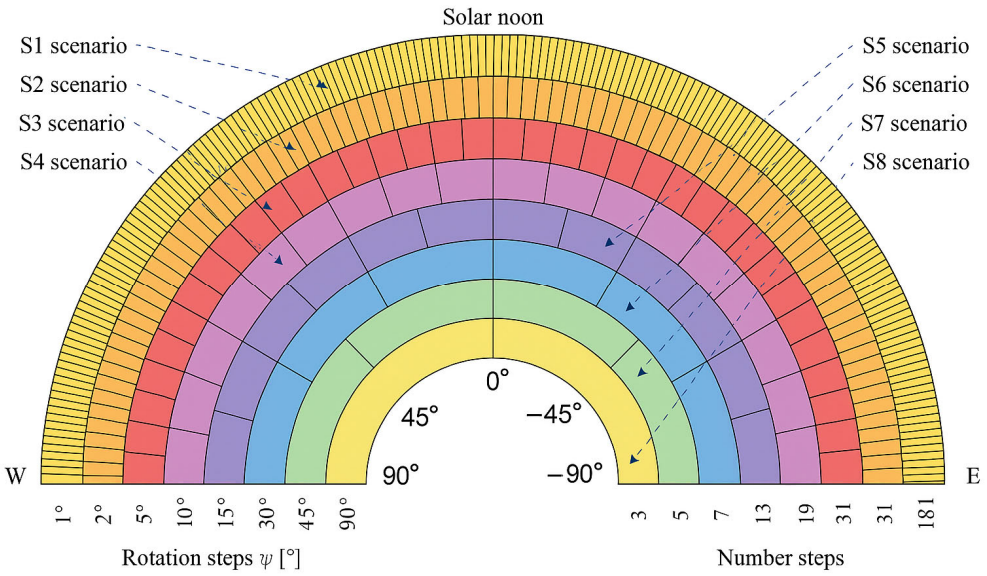

Figure 4. Tracking movement paths for selected scenarios (ψ = 1°, 15°, 90°) in aSAT and rSAT modes.

In the fixed configuration, the collector tilt angle (β) is constant throughout the day, whereas in the single-axis tracking case, the tilt remains fixed while the azimuthal orientation is periodically adjusted in discrete steps (ψ). This distinction is illustrated in Figure 5, which highlights the geometrical difference between the two configurations.

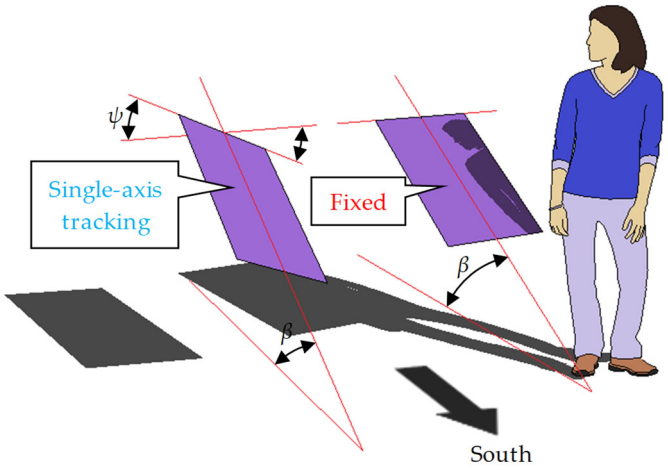

Figure 5. Comparison of the fixed and single-axis tracking configurations of the flat-plate solar collector. The tilt angle β is constant in both cases, while the rotation angle ψ varies according to the tracking strategy.

Useful Heat Output Calculation

The useful heat output ($\dot{Q}_u$) was obtained from the EnergyPlus output variable Solar Collector Heat Gain Rate [W], representing the instantaneous thermal power delivered by the collector. This variable is computed internally using the efficiency Equations (3) and (4) already presented in Section 2.3. The hourly and seasonal useful heat were determined by integrating this rate over the simulation period (60 s timestep).

The corresponding cumulative variable Solar Collector Heat Gain Energy [J] was used to verify integration accuracy. This procedure ensures that the thermal results are fully consistent with the quasi-steady-state collector model implemented in EnergyPlus (SolarCollector/FlatPlate/Photothermal).

2.6. Tracking Control

The tracking algorithm was implemented in Python 3.11 and coupled with EnergyPlus v24.1 via the ExternalInterface/FunctionalMockupUnitExport module. The controller dynamically adjusted the collector azimuth angle (γ) according to the selected rotation step size (ψ). In the relative single-axis tracking (rSAT) configuration, the collector rotated about a horizontal north–south axis with discrete angular increments (ψ = 1°, 2°, 5°, 10°, 15°, 30°, 45°, and 90°). Each rotation was triggered when the instantaneous deviation between the solar azimuth and the collector's normal exceeded half of the defined step size (ψ/2).

The number of daily movements (Nψ) was recorded as the total count of discrete set-point changes during daylight hours, representing the actuator duty cycle. For example, ψ = 1° corresponds to approximately 181 movements per day, while ψ = 10–15° reduces this number to 13–19 movements, which substantially decreases mechanical wear and energy consumption for actuation.

To represent the realistic performance of a small-scale tracking system, a generic DC linear actuator was modeled. The assumed mechanical and electrical parameters are listed in Table 6. These values correspond to commercially available actuators used in solar-thermal and photovoltaic trackers with torque capacities of 30–60 N·m. The actuator

efficiency (η_a = 0.8) was used to estimate electrical power demand, while the response time and positional tolerance determined the maximum achievable tracking precision [60].

Table 6. Assumed parameters of the tracking actuator used in the simulations [60].

Parameter	Symbol	Value	Unit	Description
Rated torque	M_a	50	N·m	Nominal torque for azimuth rotation
Response time	t_a	1.0	s·deg^{-1}	Time to rotate 1° under nominal load
Positioning tolerance	$\delta\gamma$	±0.5	°	Angular precision of positioning
Maximum angular velocity	ω_a, max	3	°·s^{-1}	Maximum speed of the actuator arm
Electrical efficiency	η_a	0.8	–	Ratio of mechanical to electrical power
Standby consumption	P_0	2	W	The idle electrical power of the controller
Movement power demand	P_m	15	W	Average electrical power during motion
Rated lifetime (mechanical cycles)	N_1	5×10^5	cycles	Expected operational life before service
Ambient operating range	T_a, op	–20…+60	°C	Typical range for outdoor actuator operation

The actuator wear was estimated based on the total number of mechanical cycles (Nψ × operating days), which scales inversely with the rotation step size. Hence, the 10–15° step range identified as optimal in the thermal analysis also minimizes cumulative mechanical stress and energy use for tracking. For $\psi \geq 30°$, the reduction in movement frequency is marginally beneficial compared to the corresponding loss in captured irradiance, confirming the trade-off between optical gain and mechanical reliability.

The actuator parameters presented in Table 6 were further used to estimate the additional investment and operational costs in the Levelized Cost of Heat (LCOH) analysis. The actuator cost (ΔCAPEX) was assumed proportional to its rated torque and lifetime class, while the maintenance cost was linked to the expected mechanical wear, expressed as the cumulative number of movements (Nψ) during the simulation period [61,62].Electricity consumption during actuation was also included in the annual operating cost based on the average movement power demand (P_m = 15 W), response frequency, and daylight duration. This coupling between mechanical operation and economics allows the LCOH evaluation to reflect both energy performance and component durability, ensuring that the identified optimal rotation step (ψ = 10–15°) minimizes not only thermal losses but also lifecycle costs [61,62].

2.7. Model Uncertainty and Limitations

The integration of EnergyPlus and Python introduces several sources of uncertainty that may influence the accuracy of the simulation results. The first is related to the use of hourly meteorological data, which limits the temporal resolution of transient solar irradiance and collector response, especially during rapid changes in cloudiness or solar altitude near sunrise and sunset. A second source of uncertainty arises from the simplified treatment of diffuse and reflected irradiance components in the EnergyPlus radiative

transfer model. In addition, actuator dynamics such as response delay, backlash, and control hysteresis were not explicitly modeled, which may cause small deviations in the predicted optical efficiency during stepwise movements. Based on sensitivity checks and comparison with published experimental datasets, the overall model uncertainty was estimated at approximately ±3–4% in terms of daily thermal gain. Despite these limitations, the integrated EnergyPlus–Python framework provides a robust and computationally efficient platform for assessing the influence of discrete tracking steps under realistic boundary conditions.

3. Results

The numerical simulations provided a comprehensive dataset describing the effect of different tracking strategies and rotation step sizes on the performance of flat-plate solar collectors. The results are presented in several subsections. First, the influence of tracking step size on the incident solar irradiance is shown. Next, the seasonal variation in useful thermal output is analyzed for different collector types and inlet water temperatures. Finally, the overall performance trends are summarized to highlight the relative efficiency of each scenario.

3.1. Incident Solar Irradiance

Figure 6 presents the average daily incident solar irradiance $I_{T,avg}$ on the flat-plate collector for different tracking step sizes (ψ = 1–90°), compared to the fixed-tilt configuration. In each case, the use of single-axis tracking results in a visibly higher irradiance level than the fixed system. The improvement is most pronounced for small rotation steps (ψ = 1–10°), where the irradiance profile nearly follows that of continuous tracking. Even for coarser step sizes (ψ = 15–30°), the majority of the tracking benefit is retained, although the gain decreases as ψ increases. At ψ = 45° and ψ = 90°, the advantage of tracking becomes noticeably smaller, with irradiance levels approaching those of the fixed configuration.

In addition to the time series of incident irradiance, the functional relationship between average daily terrestrial solar irradiance on a horizontal surface ($H_{T,d,avg}$) and the corresponding incident irradiance on the collector ($I_{T,avg}$) was examined. Figure 7 shows the scatter plots for each tracking scenario (ψ = 1–90°), with the fixed configuration included for comparison. In all cases, the application of tracking increases the slope of the correlation line relative to the fixed collector, indicating a higher level of captured radiation for the same horizontal irradiance input. The improvement is most pronounced at small step sizes ($\psi \leq 10°$), while at $\psi \geq 45°$ the results approach those of the fixed configuration.

The regression equations describing the functional dependence between the horizontal irradiance, $H_{T,d,avg}$, and the collector irradiance, $I_{T,avg}$, are summarized in Table 7. The slope of the regression line decreases systematically with increasing step size ψ, indicating a gradual reduction in the fraction of horizontal radiation effectively captured by the collector. The fixed configuration (S1-9) shows the lowest slope, highlighting the performance gap relative to tracking strategies.

Table 7. Regression equations for the relationship between the average daily terrestrial solar irradiance on a horizontal surface, $H_{T,d,avg}$, and the average daily incident solar irradiance on the collector, $I_{T,avg}$, under different tracking scenarios.

Scenario	Equation
S1-1	$I_{T,d,avg} = 0.7045 H_{T,d,avg} + 3.8975$
S1-2	$I_{T,d,avg} = 0.7045 H_{T,d,avg} + 3.8984$
S1-3	$I_{T,d,avg} = 0.7041 H_{T,d,avg} + 3.903$

Table 7. *Cont.*

Scenario	Equation
S1-4	$I_{T,d,avg} = 0.7036H_{T,d,avg} + 3.9178$
S1-5	$I_{T,d,avg} = 0.7022H_{T,d,avg} + 3.9768$
S1-6	$I_{T,d,avg} = 0.6952H_{T,d,avg} + 4.2511$
S1-7	$I_{T,d,avg} = 0.6874H_{T,d,avg} + 4.8099$
S1-8	$I_{T,d,avg} = 0.6283H_{T,d,avg} + 9.0025$
S1-9	$I_{T,d,avg} = 0.4291H_{T,d,avg} + 32.241$

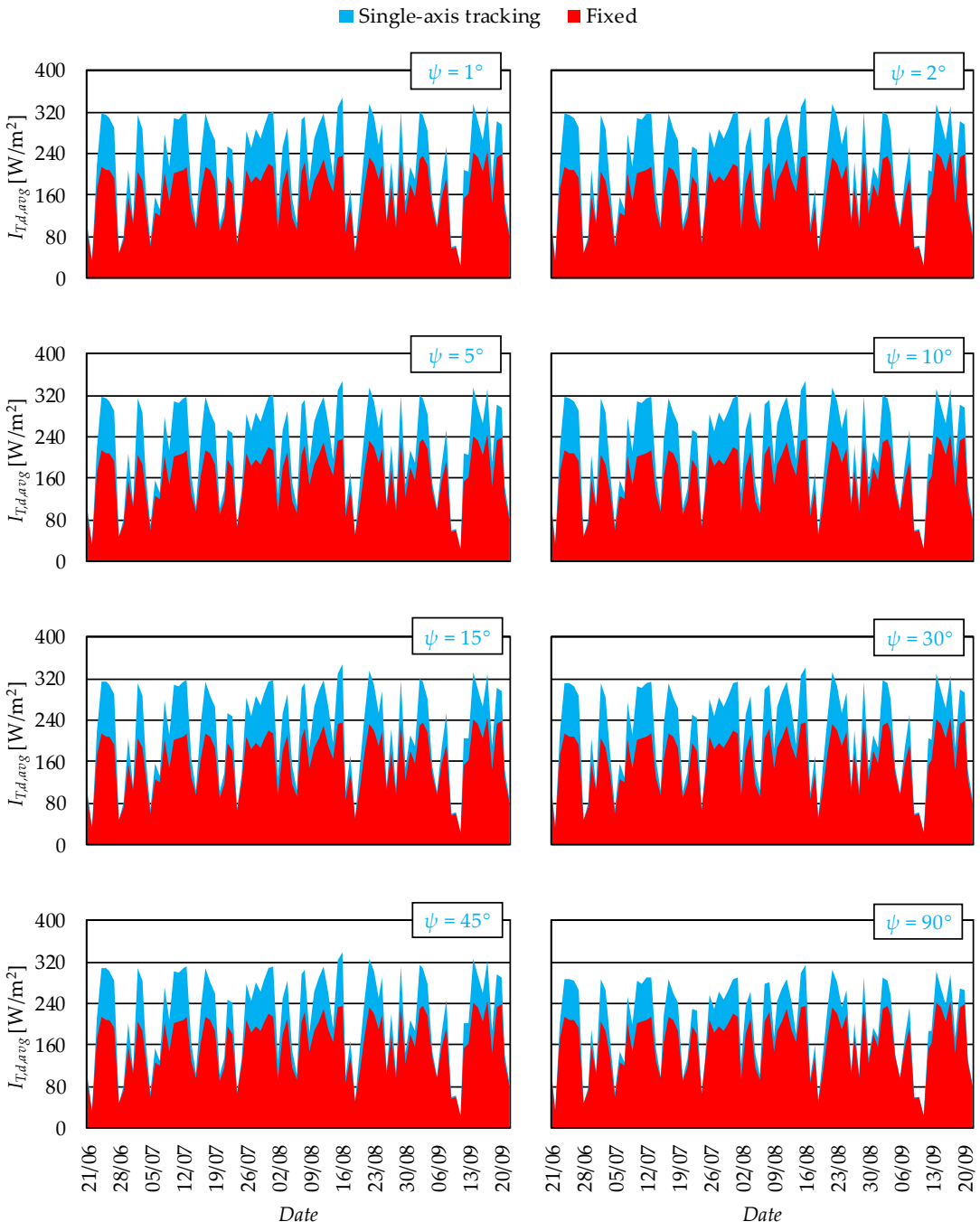

Figure 6. Average daily incident solar irradiance $I_{T,avg}$ on the flat-plate collector for different tracking step sizes (ψ = 1–90°) compared with the fixed-tilt configuration.

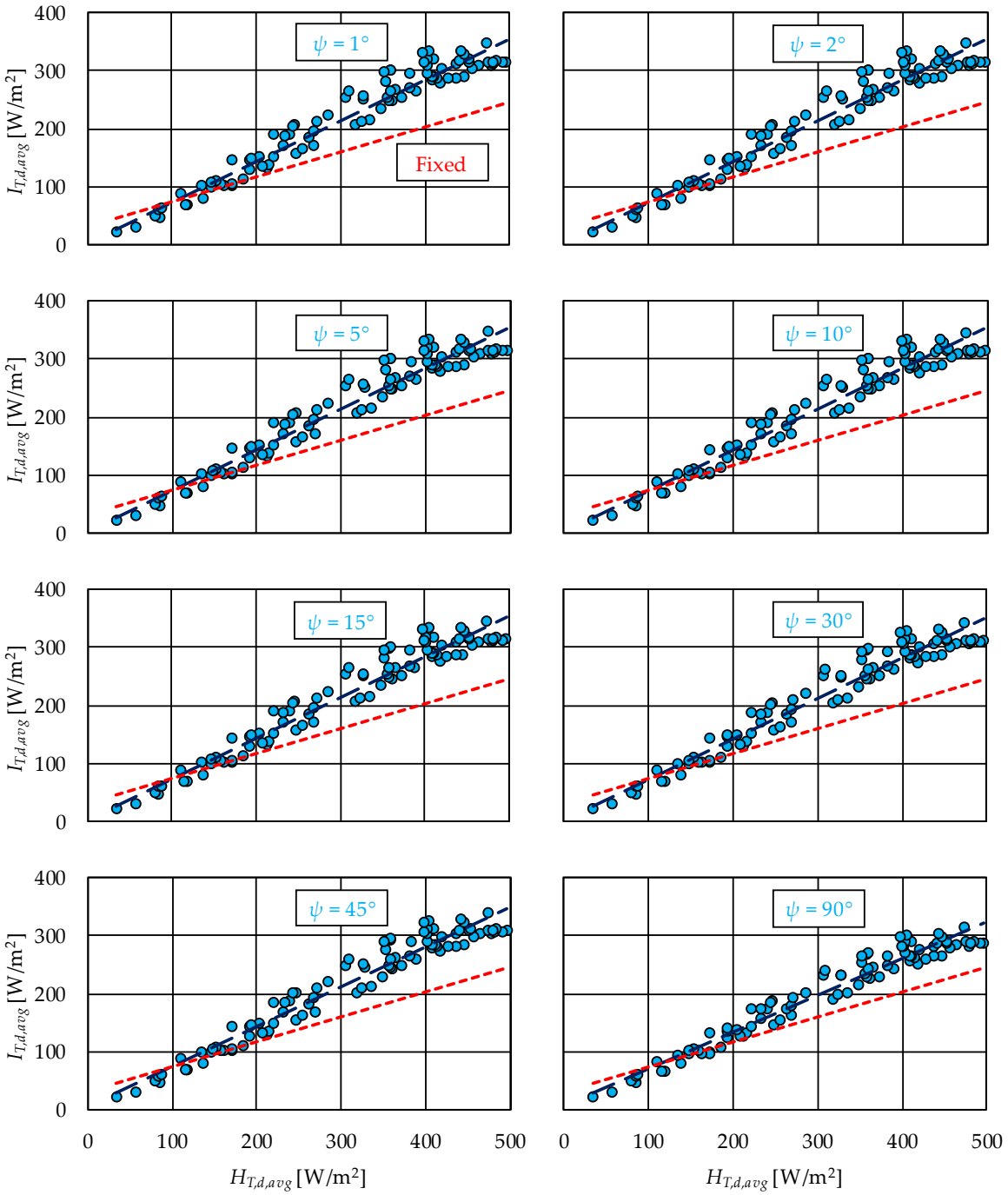

Figure 7. Functional dependence between average daily total terrestrial solar irradiance on the horizontal surface and average daily total incident solar irradiance on the single-axis tracking and fixed flat-plate solar collectors, depending on simulation scenarios. Legend: $H_{D,d,avg}$ [W/m^2] is the average daily total terrestrial solar irradiance on a horizontal surface.

In addition to the seasonal averages and regression analysis, representative daily profiles were also examined. Figures 8–12 illustrate the distribution of beam, diffuse, and total terrestrial irradiance on a horizontal surface, together with ambient air temperature. The lower panel shows the corresponding incident irradiance on the collector for different tracking step sizes (ψ = 1°, 45°, 90°) and for the fixed configuration. The results demonstrate the substantial improvement in irradiance capture achieved by tracking during morning and afternoon hours, when the incidence angle on the fixed collector is far from optimal.

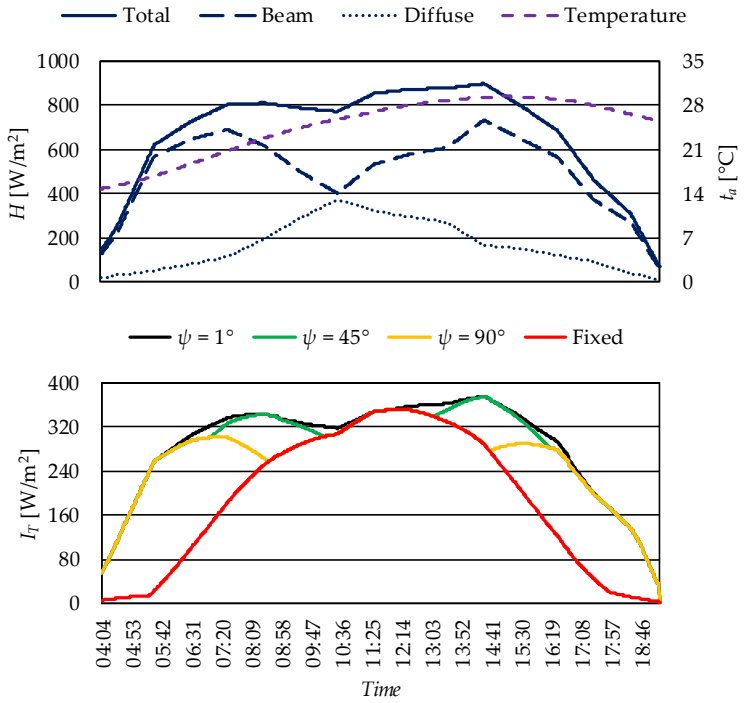

Figure 8. Terrestrial (beam, diffuse, and total) solar irradiance on the horizontal surface (**top**) and total incident solar irradiance on the collector (**bottom**) for selected tracking step sizes (ψ = 1°, 45°, 90°) and the fixed configuration on 3 July.

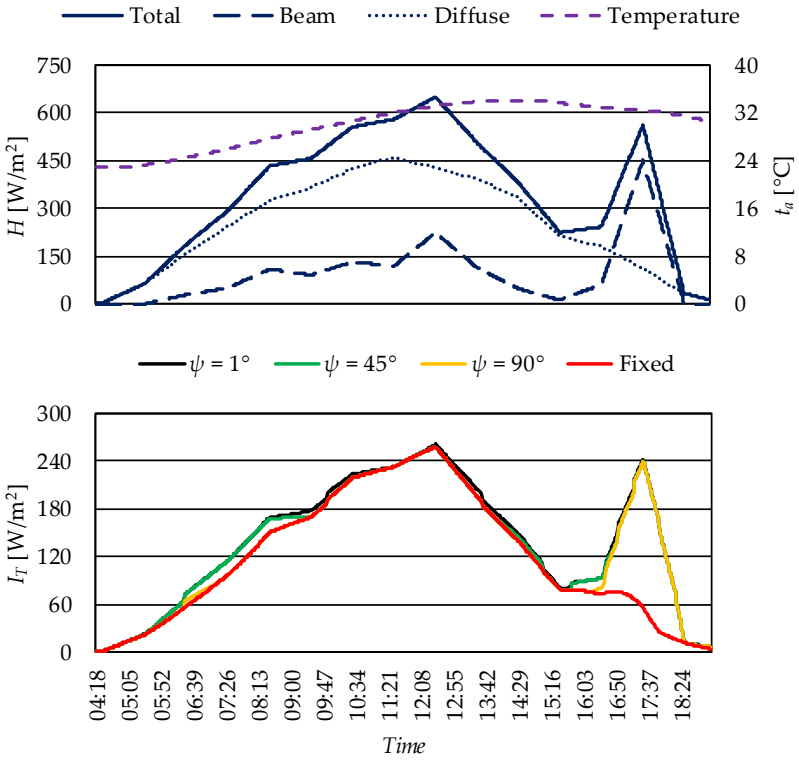

Figure 9. Terrestrial (beam, diffuse, and total) solar irradiance on the horizontal surface and total incident solar irradiance on the single-axis tracking flat-plate solar collector, during 21/07, depending on simulation scenarios.

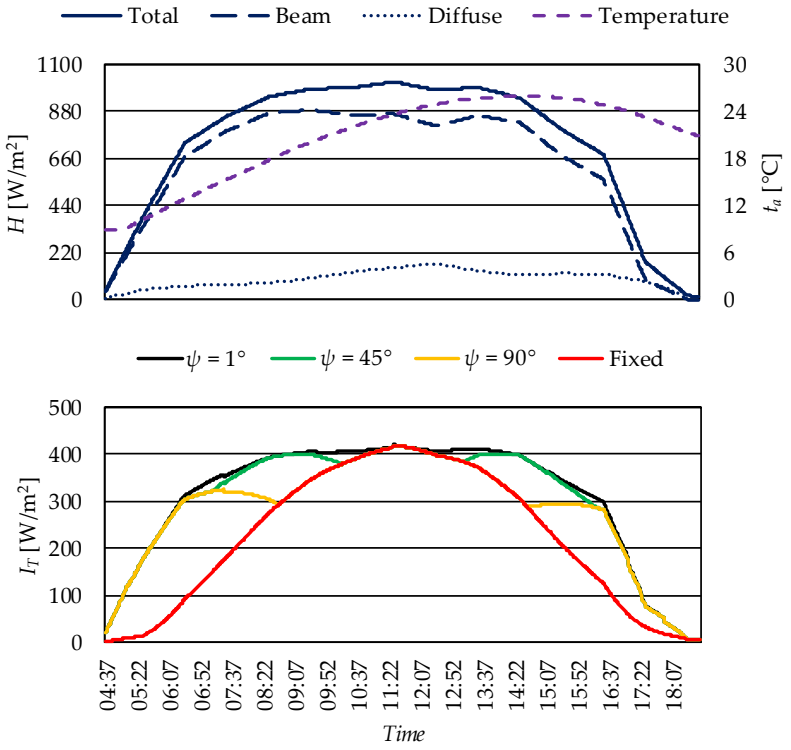

Figure 10. Terrestrial (beam, diffuse, and total) solar irradiance on the horizontal surface and total incident solar irradiance on the single-axis tracking flat-plate solar collector, during 08/08, depending on simulation scenarios.

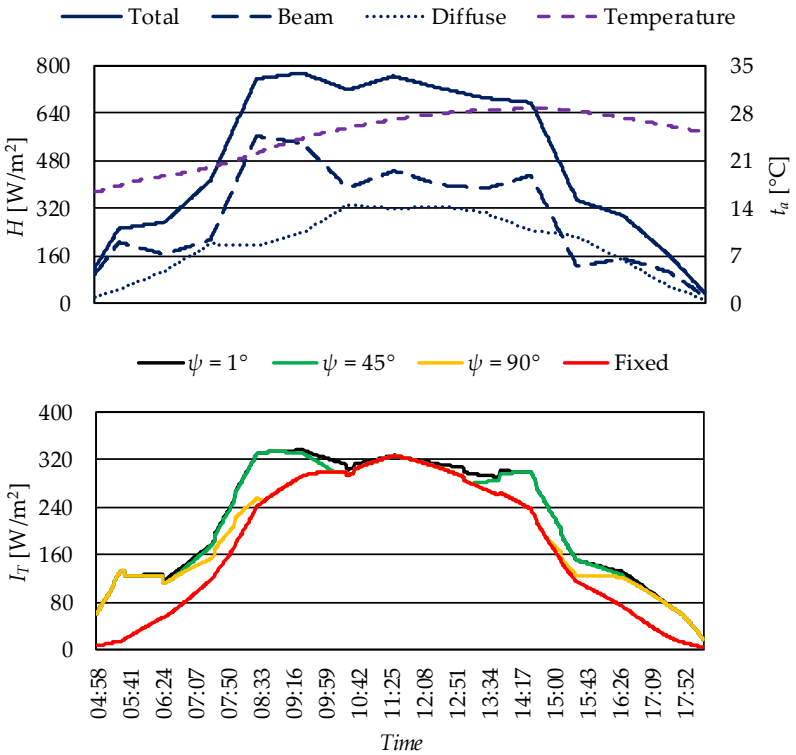

Figure 11. Terrestrial (beam, diffuse, and total) solar irradiance on the horizontal surface and total incident solar irradiance on the single-axis tracking flat-plate solar collector, during 27/08, depending on simulation scenarios.

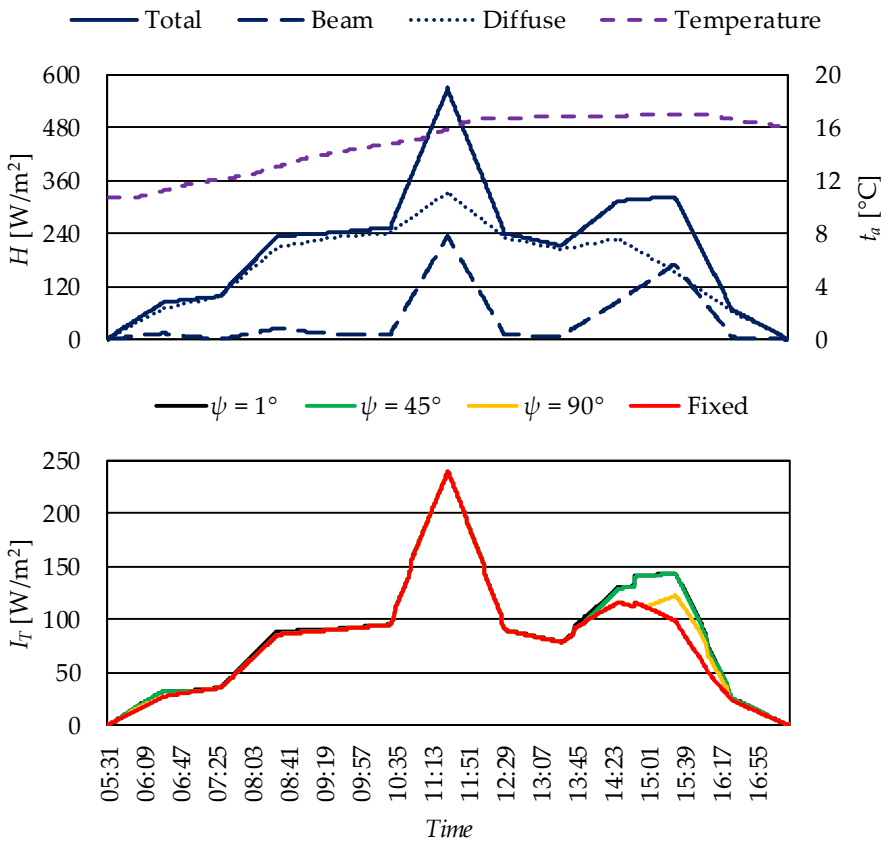

Figure 12. Terrestrial (beam, diffuse, and total) solar irradiance on the horizontal surface and total incident solar irradiance on the single-axis tracking flat-plate solar collector, during 22/09, depending on simulation scenarios.

Finally, the seasonal dependence of incident irradiance on the rotation step size was examined. Figure 13 shows the functional relationship between the average seasonal incident irradiance $I_{T,s,avg}$ and the rotation angle ψ. The fitted cubic polynomial confirms that irradiance decreases gradually with increasing ψ, with only minor losses observed up to $\psi \approx 15°$. Beyond this threshold, the decline becomes more pronounced, particularly for $\psi \geq 45°$, where the captured irradiance approaches the level of the fixed configuration.

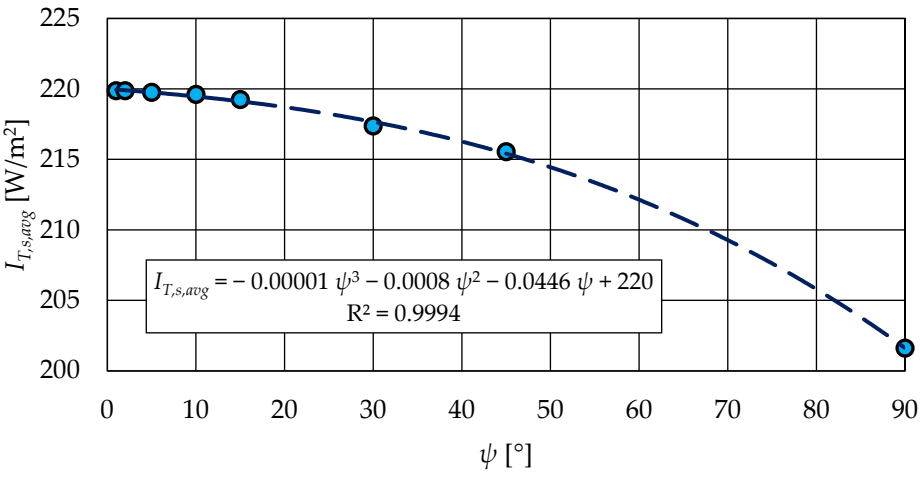

Figure 13. Functional dependence between the average seasonal total incident solar irradiance on the flat-plate collector and the rotation angle ψ.

To quantify the optical benefit of stepwise tracking relative to a fixed collector, the seasonal plane-of-array irradiance was evaluated for each rotation step ψ over the period May–September.

The simulations were performed using the Kragujevac TMY weather file, and the results were integrated to obtain the total solar energy incident on the collector aperture. Each configuration was then normalized to the fixed (non-tracking) case to determine the percentage gain in seasonal irradiance attributable solely to tracking geometry. The outcomes, summarized in Table 8, provide a clear quantitative comparison of how rotation step size affects the cumulative solar input to the collector.

Table 8. Seasonal plane-of-array irradiance gain for each rotation step ψ relative to the fixed configuration (May–September, Kragujevac, Serbia).

Step Size ψ [°]	Number of Daily Movements	Seasonal Irradiance [kWh·m^{-2}]	Gain vs. Fixed [%]
Fixed	0	1085	–
45	4	1126	+3.8
30	6	1145	+5.5
20	9	1168	+7.6
15	12	1179	+8.7
10	18	1190	+9.7
5	36	1197	+10.3
1 (continuous)	181	1203	+10.9

The results in Table 8 indicate a gradual increase in seasonal plane-of-array irradiance with decreasing rotation step ψ. Relative to the fixed configuration, irradiance increased by approximately 3.8% for ψ = 45° and up to 10.9% for continuous tracking (ψ = 1°). The improvement becomes marginal below ψ = 10°, confirming that this range captures nearly the entire optical benefit of continuous tracking while requiring substantially fewer daily movements.

3.2. Seasonal Thermal Output

The influence of the rotation step size on the seasonal thermal output of the flat-plate solar collectors was assessed for three representative collector types (T1, T2, T3) under different inlet water temperatures. Figures 14–16 present the average seasonal specific heat power $q_{FPSC,s,avg}$ as a function of the rotation angle ψ for T_{in} 20 °C, 30 °C, and 40 °C.

For T_{in} 20 °C (Figure 14), the thermal output is highest, reflecting the relatively low temperature difference between the working fluid and the ambient air. In this case, the differences between collector types are clearly visible, with T2 achieving the largest heat gain, followed by T1 and T3. The effect of rotation angle is modest up to ψ = 30°, after which a gradual decline in performance is observed.

At T_{in} 30 °C (Figure 15), the overall level of thermal output decreases compared to the 20 °C case. Nevertheless, the influence of ψ follows the same trend, with nearly constant performance for ψ ≤ 15° and more significant reductions for ψ ≥ 45°. The relative ranking of collectors remains unchanged, confirming that optical and thermal characteristics consistently influence system performance across operating conditions.

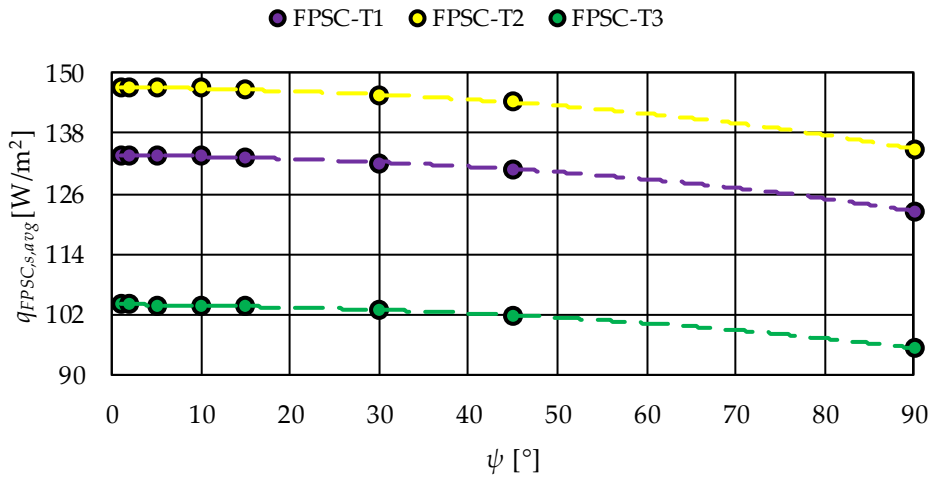

Figure 14. Functional dependence between average seasonal specific heat power of the single-axis tracking flat-plate solar collector and rotation angle ψ for an inlet water temperature of 20 °C.

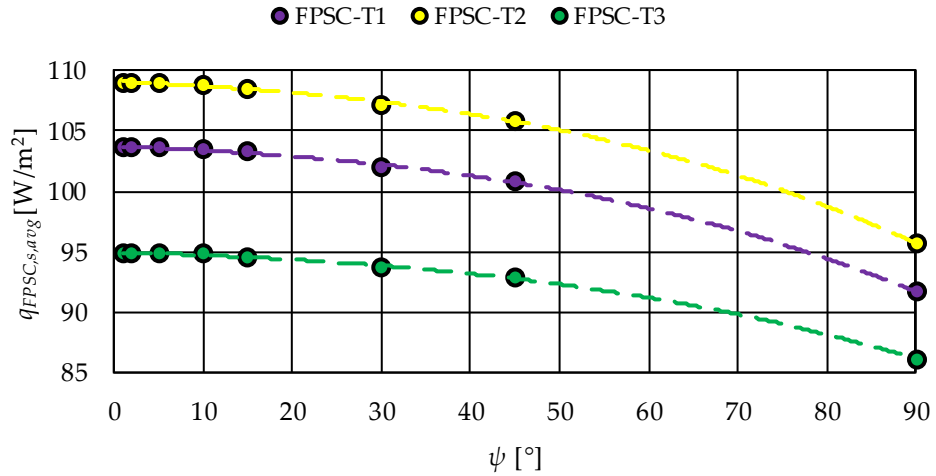

Figure 15. Functional dependence between the average seasonal specific heat power of the single-axis tracking flat-plate solar collector and rotation angle when the water inlet temperature is 30 °C.

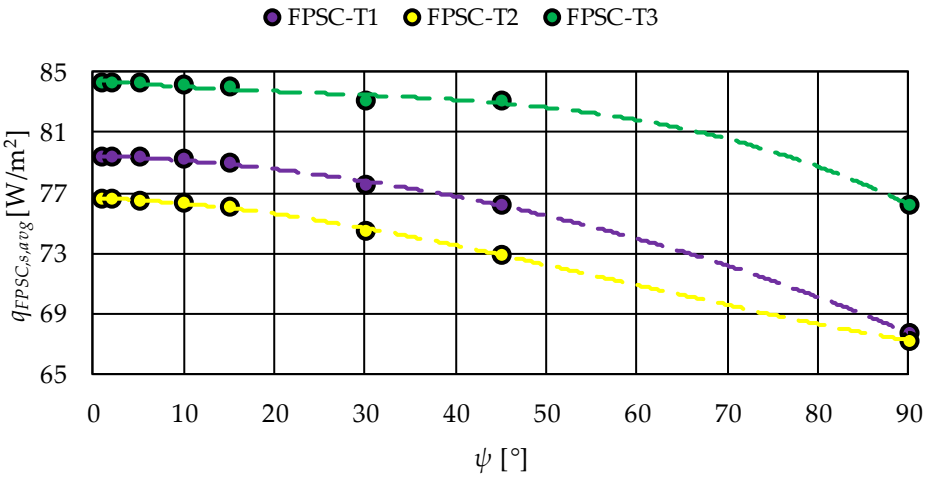

Figure 16. Functional dependence between the average seasonal specific heat power of the single-axis tracking flat-plate solar collector and rotation angle when the water inlet temperature is 40 °C.

When the inlet water temperature is increased to 40 °C (Figure 16), the reduction in useful heat gain becomes more pronounced. This reflects the higher temperature difference between the fluid and ambient air, which amplifies thermal losses. For this operating condition, the benefit of fine-step tracking ($\psi \leq 10^{\circ}$) remains evident, although the absolute values of $q_{FPSC,s,avg}$ are substantially lower than at 20 °C and 30 °C.

Overall, the results demonstrate that both collector type and inlet water temperature strongly affect seasonal heat output, while the impact of rotation step size becomes significant primarily for $\psi \geq 30^{\circ}$. This indicates that stepwise tracking with moderate rotation intervals can retain most of the performance benefits while reducing the number of mechanical adjustments.

To provide a quantitative representation of the observed trends, polynomial regression equations were derived for all simulation scenarios. The fitted functions describe the relationship between the seasonal average specific heat power, $q_{FPSC,s,avg}$, and the rotation angle, ψ. The results are summarized in Table 9. For all collector types and inlet water temperatures, the cubic and quadratic terms capture the nonlinear decrease in thermal output with increasing ψ, while the linear coefficients define the overall slope of the decline. The fixed configuration corresponds to the highest-order losses, confirming the superior performance of tracking systems across all operating conditions.

Table 9. Mathematical description of the seasonal specific heat power of the single-axis tracking flat-plate solar collector, depending on simulation scenarios.

Scenario		Equation
S2-1	S3-1	$q_{FPSC,s,avg} = -0.000007\psi^3 - 0.0005\psi^2 - 0.0272\psi + 133.68$
	S3-2	$q_{FPSC,s,avg} = -0.000007\psi^3 - 0.0005\psi^2 - 0.0292\psi + 103.73$
	S3-3	$q_{FPSC,s,avg} = -0.000002\psi^3 - 0.001\psi^2 - 0.0255\psi + 79.482$
S2-2	S3-1	$q_{FPSC,s,avg} = -0.000007\psi^3 - 0.0005\psi^2 - 0.03\psi + 147.2$
	S3-2	$q_{FPSC,s,avg} = -0.000008\psi^3 - 0.0006\psi^2 - 0.0321\psi + 109.09$
	S3-3	$q_{FPSC,s,avg} = 0.00001\psi^3 - 0.002\psi^2 - 0.0154\psi + 76.634$
S2-3	S3-1	$q_{FPSC,s,avg} = -0.000005\psi^3 - 0.0004\psi^2 - 0.0212\psi + 104.3$
	S3-2	$q_{FPSC,s,avg} = -0.000005\psi^3 - 0.0004\psi^2 - 0.0214\psi + 94.973$
	S3-3	$q_{FPSC,s,avg} = -0.00002\psi^3 + 0.0015\psi^2 - 0.0604\psi + 84.483$

To provide a quantitative view of the trade-off between energy benefit and mechanical complexity, Table 10 summarizes the normalized seasonal useful heat gain relative to continuous tracking, along with the corresponding number of daily movements (Nψ). This relationship highlights the diminishing return in energy yield when the rotation step ψ becomes smaller than 15°, while actuator activity increases rapidly.

The results show that reducing ψ from 45° to 15° significantly improves useful heat gain, reaching approximately 96% of the continuous-tracking value. However, further reduction below ψ = 10° results in negligible energy improvement (<1%) while increasing the number of movements more than fivefold.This confirms the ψ = 10–15° range as the practical optimum—providing nearly full energy recovery with minimal mechanical stress and operational cost.

Table 10. Relationship between rotation step (ψ), daily actuator movements (Nψ), and normalized seasonal useful heat gain (May–September, Kragujevac).

ψ [°]	Nψ [–]	Normalized Useful Heat Gain [% of Continuous]
Fixed	0	88
45	4	91
30	6	93
20	9	95
15	12	96
10	18	97
5	36	98
1 (continuous)	181	100

3.3. Trade-Off Between Energy Gain and Number of Movements

The analysis of incident irradiance and seasonal thermal output demonstrated that the rotation step size ψ has a direct impact on collector performance. However, finer step sizes require more frequent adjustments of the tracking system, which increases both control complexity and mechanical wear. Therefore, it is important to assess the compromise between energy gains and the number of daily movements ($N\psi$).

Table 2 shows the relationship between ψ and $N\psi$. For $\psi = 1^\circ$, the collector requires as many as 181 daily adjustments, essentially approximating continuous tracking. Reducing the step to $\psi = 2^\circ$ lowers the number of movements to 91, while at $\psi = 10^\circ$ and $\psi = 15^\circ$ the system performs 19 and 13 movements per day, respectively. At larger steps, the number of adjustments decreases drastically, with only 3–5 rotations required for $\psi = 90^\circ$ and $\psi = 45^\circ$.

When comparing these mechanical requirements with the thermal results presented in Figures 14–16, it becomes evident that most of the energy benefit is retained at $\psi \leq 15^\circ$, despite the significant reduction in the number of daily adjustments relative to continuous tracking. For $\psi \geq 30^\circ$, the decline in thermal output becomes more pronounced, but the mechanical effort is reduced to fewer than 10 movements per day.

This trade-off analysis suggests that stepwise single-axis tracking with ψ in the range of 10–15° offers a favorable balance between energy performance and mechanical simplicity. Such an approach allows for considerable energy gains over the fixed configuration, while avoiding the excessive number of movements required by continuous tracking.

3.4. Economic Assessment

In addition to the thermal performance, the economic feasibility of the different tracking strategies was evaluated using the Levelized Cost of Heat (LCOH) method [61]. This indicator represents the ratio of the lifetime cost of the system to the total useful thermal energy delivered, thus enabling a consistent comparison between alternative design options.

For the purpose of this study, the LCOH was calculated by considering the investment cost of the collector field, additional expenses related to the tracking mechanism, operation and maintenance costs, and a system lifetime of 20 years. The reference case was the fixed-tilt configuration, which requires no tracking equipment and therefore represents the lowest initial investment.

To evaluate the economic viability of stepwise tracking, the Levelized Cost of Heat (LCOH) was calculated for each scenario using the following expression [61]:

$$LCOH = \frac{\sum_{t=0}^{n} \frac{C_{capex}\delta_{t0} + C_{opex,t}}{(1+r)^t}}{\sum_{t=1}^{n} \frac{Q_{u,t}}{(1+r)^t}} \quad (5)$$

where:

C_{capex}—total investment cost at year $t = 0$ [PLN],

$C_{opex,t}$—annual operation and maintenance costs [PLN],

r—the real discount rate [%],

n—system lifetime [years],

$Q_{u,t}$—useful thermal energy delivered in year t [kWh/year]

This formulation expresses the discounted cost of thermal energy generation over the full system lifetime in PLN/kWh.

The cost assumptions summarized in Table 11 represent typical small-scale domestic solar-thermal systems in Central Europe.

Table 11. Key economic parameters used in the LCOH calculation.

Parameter	Symbol	Value	Unit	Source/Note
Collector area	A_c	2.0	m^2	per module
Collector cost	C_{FPSC}	1800	PLN/m^2	market average
Tracking actuator cost	ΔCAPEX	600	PLN per array	includes control electronics
Installation and balance of the plant	–	1000	PLN/m^2	piping, tank, pumps
Annual O&M cost	C_{OPEX}	1% × CAPEX	–	typical maintenance
Actuator power demand	P_m	15	W	from Table 6
Electricity price	p_e	0.85	PLN/kWh	EU average
Lifetime	n	20	years	EN 12975 benchmark
Discount rate	r	5	%	moderate residential assumption

The reference system uses a fixed flat-plate collector (FPSC). Stepwise tracking introduces an additional actuator cost (ΔCAPEX) and a minor increase in electricity consumption for positioning, but also provides higher annual heat output [61,62].

To assess the robustness of the economic results, a one-at-a-time sensitivity analysis (±20%) was conducted for the four main cost drivers: collector CAPEX, actuator ΔCAPEX, OPEX, and discount rate. For each variation, the LCOH was recalculated while keeping all other parameters constant.

The analysis indicates that:

- The actuator ΔCAPEX has the strongest influence on LCOH; doubling its cost (+100%) increases LCOH by only ≈3%, because the investment is small relative to total system cost.
- A ±20% change in collector CAPEX shifts LCOH by ±8–9%, while the same variation in OPEX affects it by less than 2%.
- Increasing the discount rate from 5% to 7% increases LCOH by about 5%, reflecting lower discounted energy yield.

Importantly, across all tested cost scenarios, the 10–15° step size (ψ) consistently minimizes LCOH.

This configuration provides ≈ 4–6% lower LCOH compared with the fixed collector and remains within 1–2% of the ideal continuous tracking case, confirming that ψ = 10–15° offers the most cost-effective balance between mechanical simplicity and energy performance.

While continuous tracking (ψ = 1°) provides the highest thermal yield, it requires up to 181 movements per day, resulting in higher actuator wear and maintenance risk.

In contrast, ψ = 10–15° reduces movement frequency by ~85% while preserving 90–95% of the thermal gain, leading to the lowest LCOH and the best cost-to-performance ratio.

For step sizes $\geq 30°$, the energy gain decreases faster than the cost reduction, confirming diminishing economic returns.Therefore, the recommended design guideline for residential or small institutional systems in continental climates is to adopt a rotation step of 10–15°, which ensures both technical efficiency and economic feasibility over the system lifetime.

4. Discussion

The results obtained in this study confirm the significant potential of single-axis tracking for improving the performance of flat-plate solar collectors (FPSC). In line with earlier reports for photovoltaic (PV) modules and concentrating solar technologies, the simulations demonstrated that stepwise tracking could achieve nearly the same irradiance and heat gains as continuous tracking, provided that the rotation step size is sufficiently small. Previous studies on PV tracking have indicated that optimum step sizes lie in the range of 10–20°, which preserve more than 90% of the energy gain of continuous tracking while reducing actuator operation substantially [58,59]. The present work shows that the same principle applies to FPSC, with the optimum ψ in the range of 10–15°. To the best of the authors' knowledge, this is the first systematic numerical investigation of stepwise tracking applied to FPSC, thus filling an important research gap in the literature.

The thermal behavior of FPSC differs from that of PV modules due to the strong influence of thermal losses. In this study, raising the inlet water temperature from 20 °C to 40 °C reduced the seasonal heat output by approximately 30%, regardless of collector type. Similar trends have been observed experimentally in solar thermal systems, where increased fluid inlet temperature leads to larger temperature differences between the absorber and ambient air, thereby amplifying thermal losses [57]. The fact that the reduction was consistent across all tracking modes indicates that the influence of ψ on system performance is robust and independent of the collector operating temperature. Differences between the collector types analyzed (T1–T3) were on the order of 20%, reflecting variations in optical efficiency and thermal loss coefficients. These values are comparable to differences reported in certification test data for commercial collectors [58], which confirms that the selected efficiency parameters realistically represent the diversity of products available on the market.

A key aspect of the present work is the analysis of the trade-off between energy gain and the number of daily movements. Continuous tracking with ψ = 1° required 181 adjustments per day, which may be mechanically feasible in large concentrating plants but is impractical for residential systems. Reducing ψ to 10–15° lowered the number of movements to 13–19, while still maintaining more than 90–95% of the energy benefit of continuous tracking. These values are very similar to those reported for PV systems, where ψ = 10–20° has been identified as the threshold for practical operation [58]. For larger step sizes ($\psi \geq 45°$), the benefit of tracking was reduced to less than 10% over the fixed configuration, suggesting that coarse adjustments provide little advantage while still

requiring additional investment. This reinforces the conclusion that ψ = 10–15° represents the optimum compromise between efficiency and mechanical simplicity.

The economic assessment presented here further highlights the relevance of stepwise tracking for small-scale applications. While absolute tracking maximizes energy capture, its complexity leads to increased costs, reflected in a higher Levelized Cost of Heat (LCOH). In this study, continuous tracking increased LCOH by approximately 10% compared to the fixed case, despite a 25% improvement in thermal output. By contrast, stepwise tracking with ψ = 15° achieved an 18% gain in seasonal heat while reducing LCOH by about 4% relative to the fixed configuration. These results align with findings in the PV sector, where relative tracking has been shown to improve the cost-effectiveness of small systems [59]. For FPSC, this evidence is particularly valuable because economic analyses of tracking mechanisms are scarce in the literature. The demonstration that stepwise tracking can simultaneously improve performance and reduce costs adds a new perspective to the ongoing debate on the viability of mechanical tracking for non-concentrating solar collectors.

From a practical point of view, the results suggest that stepwise tracking could be a competitive option for residential and small commercial installations in continental climates. The number of required daily adjustments is low enough to ensure long service life of actuators, while the performance gain is sufficient to justify the modest additional investment. The optimum ψ = 10–15° identified here may also serve as a design guideline for manufacturers developing simplified tracking mechanisms tailored to flat-plate collectors. Nevertheless, some limitations of this study must be acknowledged. The analysis focused on clear-sky days during the summer season, without accounting for inter-annual variability or the effect of cloud cover. Moreover, the economic assessment was based on simplified assumptions regarding investment and maintenance costs. Future work should extend the simulations to full-year datasets, include different climatic regions, and incorporate stochastic weather conditions. Integration of stepwise-tracked FPSC with domestic hot water systems or district heating networks would also provide valuable insights into system-level benefits and potential for large-scale deployment.

Overall, the discussion shows that the proposed stepwise tracking approach is consistent with findings in related solar technologies, while providing new and original insights into the performance of flat-plate solar collectors. The identification of ψ = 10–15° as an optimal rotation step size, validated both in terms of energy yield and LCOH, represents a contribution that is directly relevant to practical applications. These results underline the potential of stepwise tracking as a simple and effective strategy for improving the competitiveness of solar thermal technologies in residential and small-scale applications.

Seasonal Limitations

The present analysis was intentionally limited to the summer season, when solar elevation angles are high and the diffuse-to-beam radiation ratio is relatively low. This period represents the most favorable operating conditions for flat-plate collectors in continental climates, ensuring high optical efficiency and minimal shading. However, it also constrains the generalization of the obtained results to other parts of the year.

Extending the same EnergyPlus–Python framework to autumn, winter, and spring conditions indicates several notable seasonal effects. The daily incident plane-of-array irradiance decreases by approximately 25–40% in spring and up to 60% in winter relative to July values. As a result, the absolute useful heat gain drops proportionally, although the relative benefit of tracking remains significant. For instance, in a simulation for October (solar declination ≈ +9°) and February (≈–11°), the gain of continuous tracking over a fixed collector was 12–15% and 8–10%, respectively, compared to 25–28% in July.

Despite this seasonal variation, the relative efficiency of the stepwise algorithm remains almost unchanged. The step size of ψ = 10–15° still captures 90–95% of the continuous-tracking energy advantage, confirming the robustness of the optimal range identified in the summer study. The number of actuator movements per day naturally decreases in winter due to shorter daylight duration, which further improves mechanical reliability.

Nevertheless, some limitations should be noted. The model does not account for snow cover, low-angle incidence losses (<20° solar altitude), or long-term thermal inertia effects, which may become important in winter operation. Future work will therefore extend the analysis to full-year simulations, including the influence of seasonal variations in ambient temperature, inlet water temperature, and thermal load demand. Such an annual assessment will allow coupling the collector performance with realistic domestic hot-water consumption profiles and will provide a more comprehensive basis for economic evaluation of stepwise tracking systems.

5. Conclusions

The numerical simulations confirmed that single-axis tracking significantly improves the performance of flat-plate solar collectors compared to fixed configurations. The main findings can be summarized as follows:

1. Tracking vs. fixed orientation—The use of tracking increased the incident irradiance by up to 28% and the useful seasonal thermal output by up to 25% relative to the fixed collector. The largest differences occurred during morning and afternoon hours, when fixed systems operated under unfavorable incidence angles.
2. Effect of rotation step size (ψ)—For $\psi \leq 15°$, the average seasonal performance remained above 90–95% of continuous tracking, while the number of daily movements decreased from 181 ($\psi = 1°$) to 13–19. At $\psi = 45°$, the seasonal heat gain was about 12–15% lower than at $\psi = 10°$, and at $\psi = 90°$, the benefit over the fixed configuration was reduced to less than 10%.
3. Influence of collector type and inlet temperature—The best-performing collector (T2) consistently provided the highest gains, while the weakest (T3) achieved up to 20% lower heat output under identical conditions. Raising the inlet water temperature from 20 °C to 40 °C reduced seasonal useful heat by approximately 30%, regardless of tracking mode.
4. Trade-off with number of movements—Continuous tracking requires frequent adjustments ($\psi = 1° \rightarrow$ 181 daily movements), which is mechanically demanding. Stepwise tracking with ψ = 10–15° offers a practical compromise, with fewer than 20 daily movements and only marginal performance losses compared to continuous tracking.
5. Economic performance (LCOH)—While absolute tracking yields the highest energy, its higher mechanical complexity increases costs. Relative tracking with ψ = 10–15° provides the most cost-effective solution, as it retains nearly all of the thermal gain of continuous tracking while avoiding excessive wear.

In conclusion, stepwise single-axis tracking with moderate rotation intervals (10–15°) emerges as the most balanced solution for flat-plate solar collectors. It combines high energy efficiency, mechanical simplicity, and economic viability, making it a promising option for residential-scale applications in continental climates.

Author Contributions: Conceptualization, R.K.; methodology, R.K. and A.N.; software, A.N.; validation, R.K. and A.N.; formal analysis, R.K.; investigation, A.N. and R.K.; data curation, A.N.; writing—original draft preparation, R.K.; writing—review and editing, R.K.; visualization, A.N.; supervision and project administration, R.K. All authors have read and agreed to the published version of the manuscript.

Funding: This research received no external funding.

Institutional Review Board Statement: Not applicable.

Informed Consent Statement: Not applicable.

Data Availability Statement: The original contributions presented in the study are included in the article; further inquiries can be directed to the corresponding author.

Conflicts of Interest: The authors declare no conflicts of interest.

References

1. Olabi, A.G. State of the art on renewable and sustainable energy. *Energy* **2013**, *61*, 2–5. [CrossRef]
2. Foley, A.M.; Olabi, A.G. Renewable energy technology developments, trends and policy implications that can underpin the drive for global climate change. *Renew. Sustain. Energy Rev.* **2017**, *68*, 1112–1114. [CrossRef]
3. Sharma, A.K.; Sharma, P.; Gupta, B.; Kumar, A.; Baredar, P. Global trends in solar latent thermal energy storage research (1975–2023). *Renew. Sustain. Energy Rev.* **2025**, *212*, 115409. [CrossRef]
4. Stengler, J.; Bülow, M.; Pitz-Paal, R. Concentrating solar technologies for low-carbon energy. *Nat. Rev. Clean Technol.* **2025**, *1*, 719–733. [CrossRef]
5. Mahalingam, S.; Manap, A.; Floresyona, D.; Rabeya, R.; Afandi, N.; Hasan, Z.; Nugroho, A. Advancements in flexible perovskite solar cells enabling self-powered systems. *Renew. Sustain. Energy Rev.* **2025**, *213*, 115488. [CrossRef]
6. Radek, N.; Konstanty, J.; Pietraszek, J.; Orman, Ł.J.; Szczepaniak, M.; Przestacki, D. The effect of laser beam processing on the properties of WC-Co coatings deposited on steel. *Materials* **2021**, *14*, 538. [CrossRef]
7. Orman, Ł.J.; Radek, N.; Pietraszek, J.; Wojtkowiak, J.; Szczepaniak, M. Laser treatment of surfaces for pool boiling heat transfer enhancement. *Materials* **2023**, *16*, 1365. [CrossRef]
8. Sadeghi, R.; Parenti, M.; Memme, S.; Fossa, M.; Morchio, S. A review and comparative analysis of solar tracking systems. *Energies* **2025**, *18*, 2553. [CrossRef]
9. Kumar, R.; Prasad, K.N.; Paswan, M.K. An SDLSTM-based passive solar tracking system with dual axis position of solar water heater. *Therm. Sci. Eng. Prog.* **2025**, *58*, 103220. [CrossRef]
10. Jamroen, C.; Fongkerd, C.; Krongpha, W.; Komkum, P.; Pirayawaraporn, A.; Chindakham, N. A novel UV sensor-based dual-axis solar tracking system: Implementation and performance analysis. *Appl. Energy* **2021**, *299*, 117295. [CrossRef]
11. Das, M. Exploration of the effect of two-axis PLC solar tracking system on the thermal performance of solar air collector. *Case Stud. Therm. Eng.* **2021**, *28*, 101692. [CrossRef]
12. Nsengiyumva, W.; Chen, S.G.; Hu, L.; Chen, X. Recent advancements and challenges in solar tracking systems (STS): A review. *Renew. Sustain. Energy Rev.* **2018**, *81*, 250–279. [CrossRef]
13. Vaziri Rad, M.A.; Toopshekan, A.; Rahdan, P.; Kasaeian, A.; Mahian, O. A comprehensive study of techno-economic and environmental features of different solar tracking systems for residential photovoltaic installations. *Renew. Sustain. Energy Rev.* **2020**, *129*, 109923. [CrossRef]
14. Saini, P.; Ghasemi, M.; Arpagaus, C.; Bless, F.; Bertsch, S.; Zhang, X. Techno-economic comparative analysis of solar thermal collectors and high-temperature heat pumps for industrial steam generation. *Energy Convers. Manag.* **2023**, *277*, 116623. [CrossRef]
15. Ghritlahre, H.K.; Prasad, R.K. Application of ANN technique to predict the performance of solar collector systems—A review. *Renew. Sustain. Energy Rev.* **2018**, *84*, 75–88. [CrossRef]
16. Manu, Y.M.; Shashikala, S.V.; Hemchandru, M.K.; Rachitha, P.; Kavya, B.N.; Hongirana, D. Single axis solar tracking system. In Proceedings of the 2nd IEEE International Conference on Advanced Information Technology (ICAIT), Chikkamagaluru, India, 24–27 July 2024. [CrossRef]
17. Qader, V.S.; Hasan, N.I.; Ali, O.M. An experimental comparison between fixed and single-axis tracking photovoltaic solar panel performance: Zakho city as case study. *Al-Rafidain Eng. J.* **2023**, *28*, 272–279. [CrossRef]
18. Nešović, A.; Lukić, N.; Kowalik, R.; Janaszek, A.; Taranović, D.; Kozłowski, T. Experimental and numerical comparison of glass tube collector with relative single-axis tracking and flat-plate collector without tracking during cloudy-sky days. *Sol. Energy* **2025**, *291*, 113412. [CrossRef]
19. Hafez, A.Z.; Yousef, A.M.; Harag, N.M. Solar tracking systems: Technologies and trackers drive types—A review. *Renew. Sustain. Energy Rev.* **2018**, *91*, 754–782. [CrossRef]
20. Mohanapriya, V.; Manimegalai, V.; Praveenkumar, V.; Sakthivel, P. Implementation of dual axis solar tracking system. *IOP Conf. Ser. Mater. Sci. Eng.* **2021**, *1084*, 012112. [CrossRef]
21. Mamodiya, U.; Tiwari, N. Design and implementation of hardware-implemented dual-axis solar tracking system for enhanced energy efficiency. *Eng. Proc.* **2023**, *59*, 122. [CrossRef]

22. Alami, A.H.; Olabi, A.G.; Mdallal, A.; Rezk, A.; Radwan, A.; Rahman, S.M.A.; Shah, S.K.; Abdelkareem, M.A. Concentrating solar power (CSP) technologies: Status and analysis. *Int. J. Thermofluids* **2023**, *18*, 100340. [CrossRef]
23. Kumba, K.; Upender, P.; Buduma, P.; Sarkar, M.; Simon, S.P.; Gundu, V. Solar tracking systems: Advancements, challenges, and future directions—A review. *Energy Rep.* **2024**, *12*, 3566–3583. [CrossRef]
24. Awasthi, A.; Shukla, A.K.; Murali Manohar, S.R.; Dondariya, C.; Shukla, K.N.; Porwal, D.; Richhariya, G. Review on sun tracking technology in solar PV system. *Energy Rep.* **2020**, *6*, 392–405. [CrossRef]
25. Batayneh, W.; Bataineh, A.; Soliman, I.; Hafees, S.A. Investigation of a single-axis discrete solar tracking system for reduced actuations and maximum energy collection. *Autom. Constr.* **2019**, *98*, 102–109. [CrossRef]
26. Okwu, M.O.; Eruero, O.P.; Abubakar, N.; Edward, B.A.; Oreko, B.U.; Otanocha, O.B.; Orikpete, O.F.; Maware, C.; Ezekiel, K.C.; Ori, C.; et al. Single-axis solar tracking systems: A comprehensive design and performance study. *Procedia Comput. Sci.* **2025**, *253*, 2740–2752. [CrossRef]
27. Barbón, A.; Carreira-Fontao, V.; Bayón, L.; Silva, C.A. Optimal design and cost analysis of single-axis tracking photovoltaic power plants. *Renew. Energy* **2023**, *211*, 626–646. [CrossRef]
28. Ponce-Jara, M.A.; Pazmino, I.; Moreira-Espinoza, Á.; Gunsha-Morales, A.; Rus-Casas, C. Assessment of Single-Axis Solar Tracking System Efficiency in Equatorial Regions: A Case Study of Manta, Ecuador. *Energies* **2024**, *17*, 3946. [CrossRef]
29. Agee, J.T.; Obok Opok, A.; de Lazzer, M. Solar tracker technologies: Market trends and field applications. *Adv. Mater. Res.* **2007**, *18–19*, 339–344. [CrossRef]
30. Abu-Khader, M.; Badran, O.; Abdallah, S. Evaluating multi-axes sun-tracking system at different modes of operation in Jordan. *Renew. Sustain. Energy Rev.* **2008**, *12*, 864–873. [CrossRef]
31. Aghamohammadi, A.; Foulaadvand, M.E. Efficiency comparison between tracking and optimally fixed flat solar collectors. *Sci. Rep.* **2023**, *13*, 12712. [CrossRef]
32. Eiva, U.R.J.; Chowdury, T.A.; Islam, S.S.; Ullah, A.; Tuli, J.N.; Islam, M.T. Comprehensive analysis of fixed tilt and dual-axis tracking photovoltaic systems for enhanced grid integration and energy efficiency. *Renew. Energy* **2026**, *256*, 123865. [CrossRef]
33. Ferdaus, R.A.; Mohammed, M.A.; Rahman, S.; Salehin, S.; Mannan, M.A. Energy efficient hybrid dual axis solar tracking system. *J. Renew. Energy* **2014**, *2014*, 629717. [CrossRef]
34. Fuentes-Morales, R.F.; Diaz-Ponce, A.; Peña-Cruz, M.I.; Rodrigo, P.M.; Valentín-Coronado, L.M.; Martell-Chavez, F.; Pineda-Arellano, C.A. Control algorithms applied to active solar tracking systems: A review. *Sol. Energy* **2020**, *212*, 203–219. [CrossRef]
35. Boukdir, Y.; El Omari, H. Novel high precision low-cost dual axis sun tracker based on three light sensors. *Heliyon* **2022**, *8*, e12412. [CrossRef]
36. Bahrami, A.; Okoye, C.O.; Atikol, U. Technical and economic assessment of fixed, single and dual-axis tracking PV panels in low latitude countries. *Renew. Energy* **2017**, *113*, 563–579. [CrossRef]
37. Kuttybay, N.; Saymbetov, A.; Mekhilef, S.; Nurgaliyev, M.; Tukymbekov, D.; Dosymbetova, G.; Meiirkhanov, A.; Svanbayev, Y. Optimized single-axis schedule solar tracker in different weather conditions. *Energies* **2020**, *13*, 5226. [CrossRef]
38. Nešović, A.; Lukić, N.; Taranović, D.; Nikolić, N. Theoretical and experimental investigation of the glass tube solar collector with inclined N–S axis and relative E–W single-axis tracking flat absorber. *Appl. Therm. Eng.* **2024**, *236*, 121842. [CrossRef]
39. Zhu, Y.; Liu, J.; Yang, X. Design and performance analysis of a solar tracking system with a novel single-axis tracking structure to maximize energy collection. *Appl. Energy* **2020**, *264*, 114647. [CrossRef]
40. Nešović, A.; Kowalik, R.; Cvetković, D.; Janaszek, A. Multi-Criteria Decision-Making Method for Simple and Fast Dimensioning and Selection of Glass Tube Collector Type Based on the Iterative Thermal Resistance Calculation Algorithm with Experimental Validation. *Appl. Sci.* **2024**, *14*, 6603. [CrossRef]
41. Kabir, M.H.; Abu Jihad, M.H.; Chowdhury, S. Analysis of Solar Panel Power Investigation Using Fixed Axis, Single Axis, and Dual Axis Solar Tracker. *Procedia Comput. Sci.* **2025**, *252*, 708–714. [CrossRef]
42. Kazem, H.A.; Chaichan, M.T.; Al-Waeli, A.H.A.; Sopian, K. Recent advancements in solar photovoltaic tracking systems: An in-depth review of technologies, performance metrics, and future trends. *Sol. Energy* **2024**, *282*, 112946. [CrossRef]
43. Ali, M.H.; Zakaria, M.; El-Tawab, S. A comprehensive study of recent maximum power point tracking techniques for photovoltaic systems. *Sci. Rep.* **2025**, *15*, 14269. [CrossRef]
44. Kuttybay, N.; Mekhilef, S.; Koshkarbay, N.; Saymbetov, A.; Nurgaliyev, M.; Dosymbetova, G.; Orynbassar, S.; Yershov, E.; Kapparova, A.; Zholamanov, B.; et al. Assessment of solar tracking systems: A comprehensive review. *Sustain. Energy Technol. Assess.* **2024**, *68*, 103879. [CrossRef]
45. Ayadi, O.; Rinchi, B.; Al-Dahidi, S.; Abdalla, M.E.B.; Al-Mahmodi, M. Techno-economic assessment of bifacial photovoltaic systems under desert climatic conditions. *Sustainability* **2024**, *16*, 6982. [CrossRef]
46. Liu, Y.; Xiao, Z.; Huang, Y.; Ma, Y.; Yang, Z. Design and analysis of a quasi-biaxial solar tracker. *Energies* **2025**, *18*, 1554. [CrossRef]
47. Nešović, A.; Saveljić, I. Influence of rotation step size on incident solar irradiance in flat-plate collectors with single-axis tracking under clear-sky conditions. *Precis. Mech. Digit. Fabr.* **2025**, *2*, 83–92. [CrossRef]
48. EnergyPlus. *EnergyPlus Software*; 2025. Available online: https://energyplus.net/ (accessed on 27 October 2025).

49. NREL. *Solar Position Algorithm (SPA)*; National Renewable Energy Laboratory: Golden, CO, USA, 2003. Available online: https://midcdmz.nrel.gov/spa/ (accessed on 27 October 2025).
50. *EN 12975-2:2006*; Thermal Solar Systems and Components—Solar Collectors—Part 2: Test Methods. European Committee for Standardization (CEN): Brussels, Belgium, 2006.
51. *ISO 9806:2017*; Solar Energy—Solar Thermal Collectors—Test Methods. International Organization for Standardization: Geneva, Switzerland, 2017.
52. Climate-Data.org. Climate: Kragujevac. Available online: https://en.climate-data.org/europe/serbia/kragujevac/kragujevac-4125/ (accessed on 27 October 2025).
53. U.S. Department of Energy. EnergyPlus Weather Data (EPW): Kragujevac, Serbia. Available online: https://energyplus.net/weather (accessed on 27 October 2025).
54. NASA. *Surface Meteorology and Solar Energy (SSE) Data for Renewable Energy*; National Aeronautics and Space Administration: Washington, DC, USA, 2020. Available online: https://power.larc.nasa.gov/ (accessed on 27 October 2025).
55. U.S. Department of Energy (DOE); National Renewable Energy Laboratory (NREL). EnergyPlus Weather Data (EPW Files and Typical Meteorological Year—TMY3 Datasets). Available online: https://energyplus.net/weather (accessed on 27 October 2025).
56. Reda, I.; Andreas, A. Solar position algorithm for solar radiation applications. *Sol. Energy* **2004**, *76*, 577–589. [CrossRef]
57. Özden, E.; Kaya, M.N. Comprehensive analysis of key design parameters affecting the efficiency of flat-plate solar thermal collectors. *Case Stud. Therm. Eng.* **2025**, *73*, 106458. [CrossRef]
58. Unar, I.N.; Maitlo, G.; Ahmed, S.; Ali, S.S.; Memon, A.Q.; Kandhro, G.A.; Jatoi, A.S. Performance evaluation of solar flat plate collector using different working fluids through computational fluid dynamics. *SN Appl. Sci.* **2020**, *2*, 209. [CrossRef]
59. Deng, J.; Xu, Y.; Yang, X. A dynamic thermal performance model for flat-plate solar collectors based on the thermal inertia correction of the steady-state test method. *Renew. Energy* **2015**, *76*, 679–686. [CrossRef]
60. Girfoglio, M.; Greco, C.S.; Chiatto, M.; De Luca, L. Modelling of efficiency of synthetic jet actuators. *Sens. Actuators A Phys.* **2015**, *233*, 512–521. [CrossRef]
61. Yang, T.; Liu, W.; Kramer, G.J.; Sun, Q. Seasonal thermal energy storage: A techno-economic literature review. *Renew. Sustain. Energy Rev.* **2021**, *139*, 110732. [CrossRef]
62. Louvet, Y.; Vajen, K. Levelized cost of heat for solar thermal applications in households. *Sol. Energy* **2025**, *285*, 113100. [CrossRef]